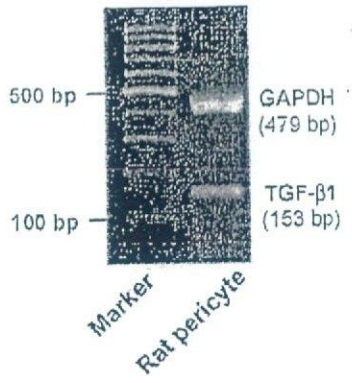

Fig. 2. TGF-β1 mRNA expression in rat pericytes detected by RT-PCR analysis. RNA samples from rat pericytes were used for RT-PCR with primer pairs specific for rat TGF-β1 and GAPDH.

significant effects for culture system [$F(1, 18) = 14.88$, $P < 0.005$] and interaction [$F(1, 18) = 11.97$, $P < 0.005$], but not for treatment. Tukey–Kramer post hoc tests indicated that anti-TGF-β1 antibody significantly increased the permeability to Na-F ($P < 0.01$) and the accumulation of rhodamine 123 in MBEC4 cells ($P < 0.05$) in the coculture system, but not in the monolayer (Fig. 3).

A 12-h exposure to SB431542 (10 μM) significantly increased the permeability from 73.8 ± 3.4 to 87.6 ± 3.9% and moderately elevated the accumulation of rhodamine 123 in MBEC4 cells from 79.0 ± 8.4 to 91.7 ± 11.6% of the control value in the opposite coculture system (Fig. 4). For permeability to Na-F (Fig. 4A), a two-way ANOVA showed significant effects for the factors culture system [$F(1, 21) = 90.10$, $P < 0.0001$], treatment [$F(1, 21) = 14.21$, $P < 0.005$] and interaction [$F(1, 21) = 6.73$, $P < 0.05$]. For the accumulation of rhodamine 123 (Fig. 4B), a two-way ANOVA showed significant effects for culture system [$F(1, 32) = 13.18$, $P < 0.001$] and interaction [$F(1, 32) = 4.16$, $P < 0.05$], but not for treatment. Tukey–Kramer post hoc tests indicated that SB431542 significantly increased the permeability to Na-F ($P < 0.01$) in the coculture system, but not in the MBEC4 monolayer.

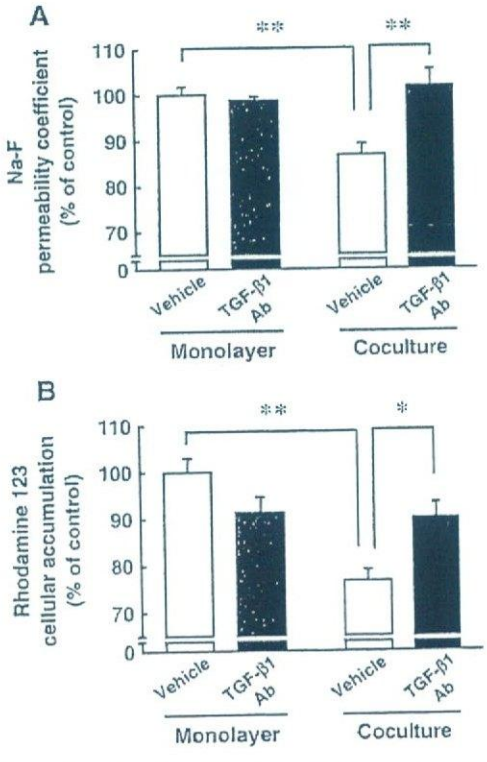

Fig. 3. Effect of anti-TGF-β1 antibody on MBEC4 permeability (A) and P-gp function of MBEC4 cells (B) in the MBEC4 monolayer and rat pericyte coculture systems. Experiments were performed after 12 h of exposure to anti-TGF-β1 antibody (TGF-β1 Ab; 10 μg/ml). (A) MBEC4 permeability coefficients of Na-F. Results are expressed as a percentage of the control (vehicle-treated MBEC4 monolayers) value ($3.85 \pm 0.11 \times 10^{-4}$ cm/min). Values are the means ± SEM ($n = 6$–11). $^{**}P < 0.01$. (B) Rhodamine 123 accumulation in MBEC4 cells. Results are expressed as a percentage of the control value (2.46 ± 0.08 nmol/mg protein). Values are the mean ± SEM ($n = 3$–7). $^{*}P < 0.05$, $^{**}P < 0.01$.

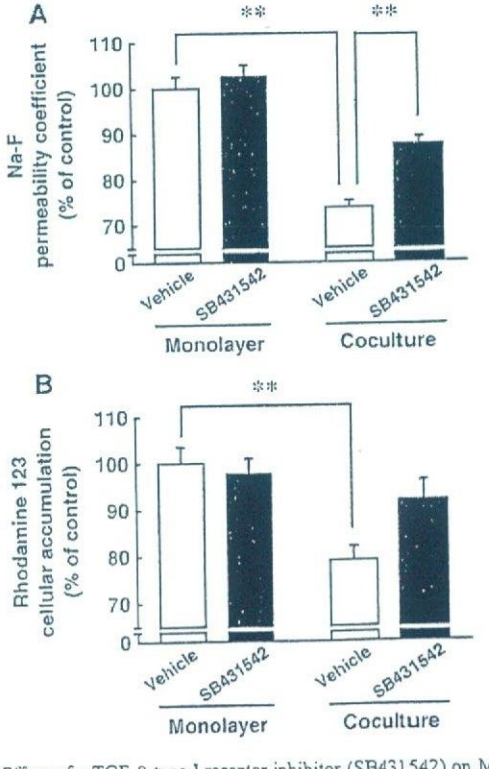

Fig. 4. Effect of a TGF-β type I receptor inhibitor (SB431542) on MBEC4 permeability (A) and P-gp function of MBEC4 cells (B) in the MBEC4 monolayer and rat pericyte coculture systems. Experiments were performed after 12 h of exposure to SB431542 (10 μM). (A) MBEC4 permeability coefficients of Na-F. Results are expressed as a percentage of the control (vehicle-treated MBEC4 monolayers) value ($4.29 \pm 0.18 \times 10^{-4}$ cm/min). Values are the means ± SEM ($n = 4$–8). $^{**}P < 0.01$. (B) Rhodamine 123 accumulation in MBEC4 cells. Results are expressed as a percentage of the control value (2.22 ± 0.43 nmol/mg protein). Values are the mean ± SEM ($n = 7$–12). $^{**}P < 0.01$.

3.3. Effect of TGF-β type I receptor antagonist on TGF-β1-induced enhancement of BBB functions in MBEC4 monolayer

To determine whether the site of treatment had an effect on the permeability of MBEC4 cells, TGF-β1 (10 ng/ml) was applied to the luminal or abluminal side of the MBEC4 monolayer. A 12-h exposure to TGF-β1, when injected into either the luminal or abluminal side, produced significant decreases with the same change in permeability to Na-F (35.7 and 36.6%, respectively) (Fig. 5). Then, TGF-β1 and the TGF-β1 receptor antagonist were applied to the luminal compartment of the MBEC4 monolayer.

The TGF-β1 antagonist SB431542 (10 μM) alone had no effect on the permeability to Na-F and the accumulation of rhodamine 123 in the MBEC4 monolayer. TGF-β1 (1 ng/ml) significantly decreased the permeability ($P < 0.01$ vs. vehicle) and accumulation of rhodamine 123 in MBEC4 cells ($P < 0.01$ vs. vehicle). SB431542 (10 μM) completely blocked the TGF-β1-induced decreases in permeability (106.5 ± 2.2% of vehicle, $P < 0.01$ vs. TGF-β1) and accumulation of rhodamine 123 (107.4 ± 4.0% of vehicle, $P < 0.01$ vs. TGF-β1) (Fig. 6).

4. Discussion

The present study demonstrated that pericytes positively retain BBB functioning through contact with brain endothelial cells and a soluble factor secreted from pericytes. We made three in vitro BBB models; the MBEC4 monolayer, rat pericyte coculture (bottom) and rat pericyte coculture (opposite) (Fig. 1). The pericyte-released substances are permitted to interact with brain endothelial cells through the pores of the insert (0.4 μm pore size) in the bottom coculture model. The opposite coculture model produces a partial contact effect in addition to the soluble factor from pericytes. In the presence of rat pericytes, the permeability to Na-F and the accumulation of rhodamine 123 in MBEC4 cells were markedly decreased (Fig. 1). A positive role for

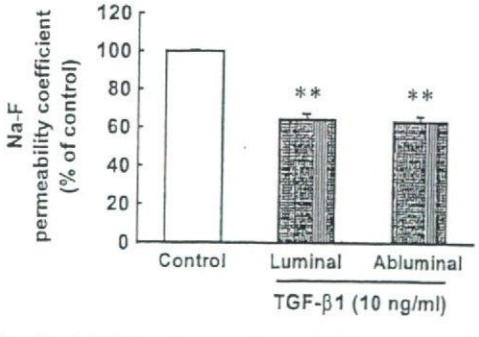

Fig. 5. Functional polarity to the permeability effect of TGF-β1 in MBEC4 monolayers. MBEC4 monolayers were exposed to TGF-β1 (10 ng/ml, 12 h) on either the luminal or abluminal side. The permeability coefficient of Na-F for the control was 2.51 ± 0.02 × 10^{-4} cm/min. Values are the mean ± SEM ($n = 4$). **$P < 0.01$, significant difference from control.

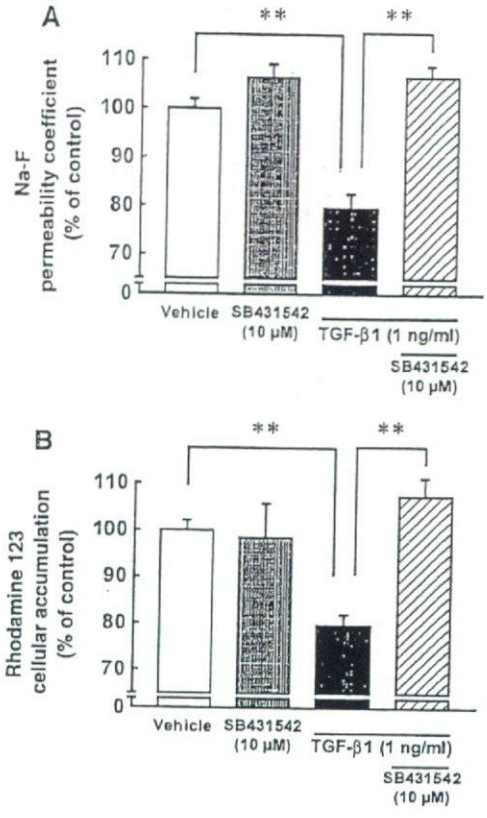

Fig. 6. Effect of a TGF-β type I receptor inhibitor (SB431542) on TGF-β1-enhanced tightening of paracellular junctions (A) and P-gp function of MBEC4 cells (B) in MBEC4 monolayers. Experiments were performed after 12 h of exposure to TGF-β1 (1 ng/ml) and/or SB431542 (10 μM). (A) MBEC4 permeability coefficients of Na-F. Results are expressed as a percentage of the control value (3.66 ± 0.25 × 10^{-4} cm/min). Values are the mean ± SEM (n = 8–12). **$P < 0.01$. (B) Rhodamine 123 accumulation in MBEC4 cells. Results are expressed as a percentage of the control value (1.14 ± 0.02 nmol/mg protein). Values are the mean ± SEM (n = 3–4). **$P < 0.01$.

pericytes in the expression and maintenance of endothelial tight junctions has been documented [13,15], although there are few reports concerning pericyte-enhanced P-gp function. Pericytes in the opposite coculture system apparently enhanced BBB properties compared to those in the bottom coculture model (Fig. 1). These findings suggest that pericytes participate in tightening the intercellular junctions and facilitating P-gp function in brain endothelial cells through the production of soluble factors and cell-to-cell contact. Therefore, we employed the opposite coculture model to investigate effects of the inhibition of TGF-β1 signaling on BBB functions in rat pericyte cocultures.

The anti-TGF-β1 antibody and TGF-β1 receptor antagonist (SB431542) were used here at the maximal concentration having no significant effect on BBB functions in the MBEC4 monolayer. Anti-TGF-β1 antibody reversed the decrease in permeability to Na-F and in the accumulation of rhodamine 123 in the rat pericyte coculture to the corresponding levels in the MBEC4 monolayer (Fig. 3). TGF-β1 receptor antagonist (SB431542) inhibited pericyte-

induced decreases in the permeability to Na-F and the accumulation of rhodamine 123 in MBEC4 cells by 50–60% (Fig. 4). A longer period of exposure than 12 h and/or an injection before 3 days may need to be tested. The present results suggest that the pericyte-induced enhancement of BBB functions is mediated to some extent by TGF-β1. RT-PCR analysis of rat pericytes demonstrated the expression of TGF-β1 (Fig. 2). It is, therefore, conceivable that pericyte-derived soluble factors include TGF-β1 and enhance both tight junctions and P-gp function through, at least in part, the TGF-β type I receptor. This notion is supported by our previous findings that TGF-β1 actually lowers the endothelial permeability and enhances the functional activity of P-gp [8]. In the present study, effects of TGF-β1 adsorption and TGF-β receptor inhibition emerged within 12 h (Figs. 3 and 4), after brain pericytes had induced a restoration of the BBB properties of MBEC4 cells. Thus, brain pericytes seem to positively maintain BBB functioning by continuously producing TGF-β1.

TGF-β expresses its physiological actions predominantly through two types of receptors with serine/threonine kinase activity, TGF-β type I and II receptors [20]. The binding of TGF-β to the TGF-β type II receptor induces the assembly of the TGF-β type I receptor-type II receptor heterodimer, leading to phosphorylation of TGF-β type I induced by the type II receptor. As shown in Fig. 6, SB431542 (10 μM) significantly inhibited the TGF-β1-induced enhancement of BBB functions in the MBEC4 monolayer, suggesting that TGF-β1 facilitates the barrier function of the BBB through the TGF-β type I receptor. It is, therefore, likely that the activation of the TGF-β1/TGF-β receptor pathway between brain endothelial cells and brain pericytes contributes to an enhancement of the tight junctions and P-gp function. Mouse brain capillary endothelial cells expressed TGF-β type I and II receptors [9]. The TGF-β type I receptor was expressed on blood vessels of the basal surface of endothelial cells [9]. In the present study, the enhancement of the permeability and P-gp function of MBEC4 cells induced by TGF-β1 (10 ng/ml) was not dependent on addition to the luminal (blood) or the abluminal (brain) side (Fig. 5). These findings suggest that the TGF-β receptor may be located on both sides of MBEC4 cells. The possibility that TGF-β1 injected into the abluminal compartment is transported in the luminal side through MBEC4 cells could not be excluded. The TGF-β signaling cascades from membrane to nucleus including MAPK and a receptor serine/threonine kinase pathway are probably involved in the enhancement of BBB functions. It is, therefore, conceivable that TGF-β facilitates the barrier function and P-gp functional activity of brain endothelial cells by increasing the expression of tight junction-associated proteins (such as occludin and claudins) and P-gp. The signal molecules involved in the enhancement of BBB functions following the activation of TGF-β1/TGF-β receptor pathway are now under investigation.

In several neurodegenerative diseases, changes in BBB functions and an increase of TGF-β1 in the brain have been described [11,16]. However, it has not been determined whether the increase in the expression of TGF-β observed in human neurodegenerative diseases is the underlying cause or the result of degenerative conditions. Thus, TGF-β1 seems to protect against impairment of the BBB and positively maintain brain homeostasis. In fact, the degeneration of pericytes was observed in neurodegenerative diseases [19,30]. This phenomenon probably decreases TGF-β production, leading to dysfunction of the BBB.

Other soluble factors derived from pericytes, VEGF and bFGF, were reported to influence BBB functions. VEGF increased the permeability of brain endothelial cells, suggesting that VEGF is a barrier-weakening factor [31]. bFGF was found to tighten the intercellular junctions and induce the expression of multidrug resistance proteins [26]. TGF-β1 up-regulated the induction of bFGF production [10]. Angiopoietin-1, an antipermeability factor [18] secreted from pericytes, produced the expression of occludin mRNA in brain endothelial cells [15]. It is, therefore, conceivable that brain pericytes regulate BBB functions by secreting these substances. TGF-β1, VEGF, bFGF and angiopoietin-1 appear to be involved in the interaction of endothelial cells, pericytes and astrocytes under physiological and pathophysiological conditions, since these substances are also produced by astrocytes.

In conclusion, brain pericytes induce and up-regulate the barrier function and P-gp functional activity of brain endothelial cells. This pericyte-induced up-regulation of BBB functions is mediated, at least in part, through continuous TGF-β production.

Acknowledgments

This work was supported, in part, by Grants-in-Aid for Scientific Research ((B)(2) 14370789) and ((C)(2) 15590475) from JSPS, Japan, by a Grant-in-Aid for Exploratory Research (16659138) from MEXT, Japan, and by funds (No. 031001) from the Central Research Institute of Fukuoka University and MEXT. HAITEKU (2000-2004). The authors thank Dr. Mária A. Deli, Institute of Biophysics, Biological Research Centre of the Hungarian Academy of Sciences for important comments on the preparation of the primary culture of pericytes.

References

[1] A. Antonelli-Orlidge, K.B. Saunders, S.R. Smith, P.A. D'Amore, An activated form of transforming growth factor β is produced by cocultures of endothelial cells and pericytes, Proc. Natl. Acad. Sci. U. S. A. 88 (1989) 4544–4548.

[2] R. Balabanov, P. Dore-Duffy, Role of the CNS microvascular pericyte in the blood–brain barrier, J. Neurosci. Res. 53 (1998) 637–644.

[3] V. Berezowski, C. Landry, M.-P. Dehouck, R. Cecchelli, L. Fenart, Contribution of glial cells and pericytes to the mRNA profiles of P-glycoprotein and multidrug resistance-associated proteins in an in vitro model of the blood–brain barrier, Brain Res. 1018 (2004) 1–9.
[4] M.M. Bradford, A rapid and sensitive method for the quantitation of microgram quantities of protein utilizing the principle of protein-dye binding, Anal. Biochem. 72 (1976) 248–254.
[5] M.-P. Dehouck, P. Jolliet-Riant, F. Brée, J.-C. Fruchart, R. Cecchelli, J.P. Tillement, Drug transfer across the blood–brain barrier: correlation between in vitro and in vivo models, J. Neurochem. 58 (1992) 1790–1797.
[6] R. Derynck, Y.E. Zhang, Smad-dependent and Smad-independent pathways in TGF-β family signaling, Nature 425 (2003) 577–584.
[7] S. Dohgu, Y. Kataoka, H. Ikesue, M. Naito, T. Tsuruo, R. Oishi, Y. Sawada, Involvement of glial cells in cyclosporine-increased permeability of brain endothelial cells, Cell. Mol. Neurobiol. 20 (2000) 781–786.
[8] S. Dohgu, A. Yamauchi, F. Takata, M. Naito, T. Tsuruo, S. Higuchi, Y. Sawada, Y. Kataoka, Transforming growth factor-β1 upregulates the tight junction and P-glycoprotein of brain microvascular endothelial cells, Cell. Mol. Neurobiol. 24 (2004) 491–497.
[9] D.B. Fee, D.L. Sewell, K. Andresen, T.J. Jacques, S. Piaskowski, B.A. Barger, M.N. Hart, Z. Fabry, Traumatic brain injury increases TGFβRII expression on endothelial cells, Brain Res. 1012 (2004) 52–59.
[10] G.A. Finlay, V.J. Thannickal, B.L. Fanburg, K.E. Paulson, Transforming growth factor-β1-induced activation of the ERK pathway/activator protein-1 in human lung fibroblasts requires the autocrine induction of basic fibroblast growth factor, J. Biol. Chem. 275 (2000) 27650–27656.
[11] K.C. Flanders, R.F. Ren, C.P. Lippa, Transforming growth factor-βs in neurodegenerative disease, Prog. Neurobiol. 54 (1998) 71–85.
[12] M. Fontaine, W.F. Elmquist, D.W. Miller, Use of rhodamine 123 to examine the functional activity of P-glycoprotein in primary cultured brain microvessel endothelial cell monolayers, Life Sci. 59 (1996) 1521–1531.
[13] K. Hayashi, S. Nakao, R. Nakaoke, S. Nakagawa, N. Kitagawa, M. Niwa, Effects of hypoxia on endothelial/pericytic co-culture model of the blood–brain barrier, Regul. Pept. 123 (2004) 77–83.
[14] K.K. Hirashi, P.A. D'Amore, Pericyte in the microvasculature, Cardiovasc. Res. 32 (1997) 687–698.
[15] S. Hori, S. Ohtsuki, K. Hosoya, E. Nakashima, T. Terasaki, A pericyte-derived angiopoietin-1 multimeric complex induces occludin gene expression in brain capillary endothelial cells through Tie-2 activation in vitro, J. Neurochem. 89 (2004) 503–513.
[16] J.D. Huber, R.D. Egleton, T.P. Davis, Molecular physiology and pathophysiology of tight junctions in the blood–brain barrier, Trends Neurosci. 24 (2001) 719–725.
[17] Y. Kim, R.Y. Imdad, A.H. Stephanson, R.S. Sprague, A.J. Lonigro, Vascular endothelial growth factor mRNA in pericytes is upregulated by phorbol myristate acetate, Hypertension 31 (1998) 511–515.
[18] S.W. Lee, W.J. Kim, Y.K. Choi, H.S. Song, H.S. Son, M.J. Son, I.H. Gelman, Y.J. Kim, K.W. Kim, SSeCKS regulates angiogenesis and tight junction formation in blood–brain barrier, Nat. Med. 9 (2003) 900–906.
[19] B.H. Liwnicz, J.L. Leach, H.-S. Yeh, M. Privitera, Pericyte degeneration and thickening of basement membranes of cerebral microvessels in complex parcial seizures: electron microscopic study of surgically removed tissue, Neurosurgery 26 (1997) 409–420.
[20] J. Massagué, TGF-β signal transduction, Annu. Rev. Biochem. 67 (1998) 753–791.
[21] A. Orlidge, P.A. D'Amore, Inhibition of capillary endothelial cell growth by pericytes and smooth muscle cells, J. Cell Biol. 105 (1987) 1455–1462.
[22] M. Ramsauer, D. Krause, R. Dermietzel, Angiogenesis of the blood–brain barrier in vitro and the function of cerebral pericytes, FASEB J. 16 (2002) 1274–1276.
[23] L.L. Rubin, J.M. Staddon, The cell biology of the blood–brain barrier, Annu. Rev. Neurosci. 22 (1999) 11–28.
[24] H.K. Rucker, H.J. Wynder, W.E. Thomas, Cellular mechanisms of CNS pericytes, Brain Res. Bull. 51 (2000) 363–369.
[25] Y. Sato, D.B. Rifkin, Inhibition of endothelial cell movement by pericytes and smooth muscle cells: activation of a latent transforming growth factor-β1-like molecular by plasmin during co-culture, J. Cell Biol. 109 (1989) 309–315.
[26] K. Sobue, N. Yamamoto, K. Yoneda, M.E. Hodgson, K. Yamashiro, N. Tsuruoka, T. Tsuda, H. Katsuya, Y. Miura, K. Asai, T. Kato, Induction of blood–brain barrier properties in immortalized bovine brain endothelial cells by astrocytic factors, Neurosci. Res. 35 (1999) 155–164.
[27] C.A. Szabó, M.A. Deli, T.K.D. Ngo, F. Joó, Production of pure primary rat cerebral endothelial cell culture: a comparison of different methods, Neurobiology 5 (1997) 1–16.
[28] T. Tatsuta, M. Naito, T. Oh-hara, I. Sugawara, T. Tsuruo, Functional involvement of P-glycoprotein in blood–brain barrier, J. Biol. Chem. 267 (1992) 20383–20391.
[29] T. Tatsuta, M. Naito, K. Mikami, T. Tsuruo, Enhanced expression by the brain matrix of P-glycoprotein in brain capillary endothelial cells, Cell Growth Differ. 5 (1994) 1145–1152.
[30] M.M. Verbeek, R.M. de Waal, J.J. Schipper, W.E. Van Nostrand, Rapid degeneration of cultured human brain pericytes by amyloid beta protein, J. Neurochem. 68 (1997) 1135–1141.
[31] W. Wang, M.J. Merrill, R.T. Borchardt, Vascular endothelial growth factor affects permeability of brain microvessel endothelial cells in vitro, Am. J. Physiol. 271 (1996) C1973–C1980.

Volume 312 Number 1 January 2005 ISSN 0022-3565

The Journal of PHARMACOLOGY And Experimental Therapeutics

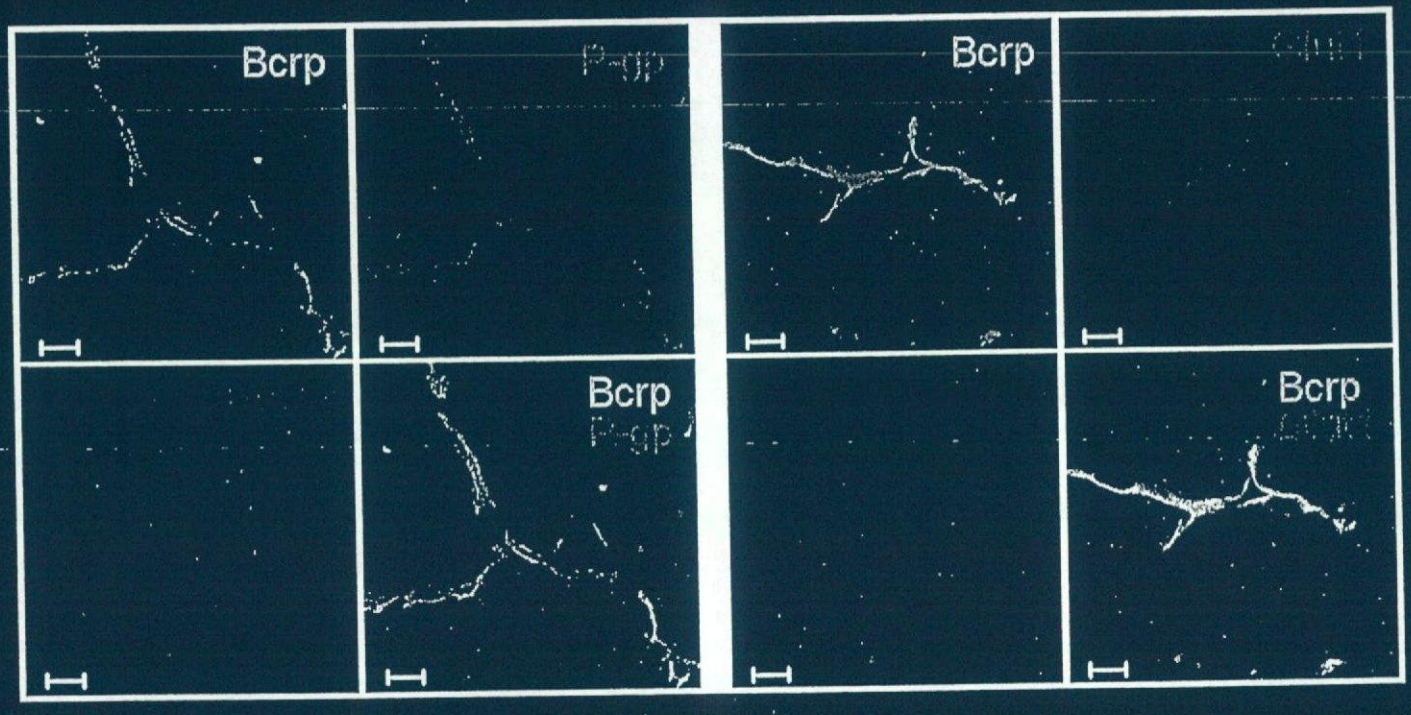

A Publication of the American Society for Pharmacology and Experimental Therapeutics

Edited for the Society by Rick G. Schnellmann

0022-3565/05/3121-44–52$20.00
THE JOURNAL OF PHARMACOLOGY AND EXPERIMENTAL THERAPEUTICS
Copyright © 2005 by The American Society for Pharmacology and Experimental Therapeutics
JPET 312:44–52, 2005

Vol. 312, No. 1
73320/1186544
Printed in U.S.A.

Investigation of Efflux Transport of Dehydroepiandrosterone Sulfate and Mitoxantrone at the Mouse Blood-Brain Barrier: A Minor Role of Breast Cancer Resistance Protein

Young-Joo Lee, Hiroyuki Kusuhara, Johan W. Jonker, Alfred H. Schinkel, and Yuichi Sugiyama

The Graduate School of Pharmaceutical Sciences, the University of Tokyo, Bunkyo-ku, Tokyo, Japan (Y.-J.L., H.K., Y.S.); and Division of Experimental Therapy, the Netherlands Cancer Institute, Amsterdam, the Netherlands (J.W.J., A.H.S.)

Received June 27, 2004; accepted September 22, 2004

ABSTRACT

Breast cancer resistance protein (Bcrp/Abcg2) is a new efflux transporter found at the blood-brain barrier (BBB) of humans and pigs. Since it has been hypothesized that Bcrp may act as a new type of efflux transporter at the BBB, we investigated the involvement of Bcrp in the efflux transport of typical substrates, dehydroepiandrosterone sulfate (DHEAS) and mitoxantrone, across the mouse BBB. The expression of Bcrp in mouse brain capillaries was confirmed by quantitative polymerase chain reaction, Western blot, and immunohistochemical analysis. The role of Bcrp as an efflux transporter was evaluated using the in situ brain perfusion method in wild-type and P-glycoprotein (P-gp) knockout mice with or without treatment with GF120918 (Elacridar), an inhibitor of both Bcrp and P-gp. The increased brain uptake of [^{3}H]DHEAS and [^{3}H]mitoxantrone by GF120918 in wild-type and P-gp knockout mice suggested the existence of a GF120918-sensitive and P-gp-independent efflux transporter for DHEAS and mitoxantrone across the BBB. However, the brain uptake of [^{3}H]DHEAS in Bcrp knockout mice was comparable with that in wild-type mice, and the effect of GF120918 was still observed in Bcrp knockout mice. In addition, the brain uptake of [^{3}H]mitoxantrone was also similar in wild-type and Bcrp knockout mice. These results suggest that although BCRP is expressed at the BBB it plays a minor role in active efflux transport of DHEAS and mitoxantrone out of brain and that one or more GF120918-sensitive efflux transporters distinct from BCRP or P-gp contributes to the brain efflux of DHEAS and mitoxantrone.

It is well known that the transport of compounds from the circulating blood into the central nervous system is restricted by the blood-brain barrier (BBB), which is formed by the brain capillary endothelial cells that are characterized by highly developed tight junctions and a paucity of fenestra and pinocytotic vesicles. In addition to these characteristics, efflux transporters expressed in the brain capillaries play an important role in the elimination of endogenous waste products and xenobiotics from the brain and prevent their accumulation in the central nervous system (Kusuhara and Sugiyama, 2001; Sun et al., 2003). Breast cancer resistance protein (BCRP/*ABCG2*) is a unique ABC efflux transporter that accepts sulfoconjugated organic anions as well as hydrophobic and amphiphilic compounds as substrates. Bcrp has been shown to restrict the intestinal absorption and fetal penetration of its substrates, such as mitoxantrone and topotecan (Allen et al., 1999; Jonker et al., 2002; Kruijtzer e al., 2002). BCRP has also been found at the luminal side o human and porcine brain capillary endothelial cells (Cooray et al., 2002; Eisenblatter and Galla, 2002; Zhang et al., 2003). Overexpression of human BCRP in immortalized rat brain endothelial cells resulted in enhanced vectorial transport of mitoxantrone, fluorescein, and rhodamine-123 in the abluminal-to-luminal direction (Zhang et al., 2003). Recently, overexpression of Bcrp in multidrug-resistance (Mdr)1a P-glycoprotein (P-gp) knockout mice has also been reported (Cisternino et al., 2004). However, it is unclear whether

This work was supported by the research grant from the Japan Foundation For Aging and Health, the Society of Japanese Pharmacopoeia, and the Minister of Health, Labor, and Welfare. Part of this study was presented at the 2004 Pharmaceutical Sciences World Congress, Kyoto, Japan; May 29–June 3, 2004.

Article, publication date, and citation information can be found at http://jpet.aspetjournals.org.
doi:10.1124/jpet.104.073320.

ABBREVIATIONS: BBB, blood-brain barrier; BCRP, breast cancer resistance protein; Mdr, multidrug-resistance; P-gp, P-glycoprotein; DHEA, dehydroepiandrosterone; DHEAS, dehydroepiandrosterone sulfate; OAT, organic anion transporter(s); OATP, organic anion-transporting polypeptide; GF120918, Elacridar; RT-PCR, reverse transcriptase-polymerase chain reaction; HPRT, hypoxanthine phosphoribosyl-transferase; Mrp, multidrug resistance-associated protein; TBST, Tris-buffered saline/Tween 20; PBS, phosphate-buffered saline; Glut, glucose transporter; BSA, bovine serum albumin; ANOVA; analysis of variance.

RP plays a role as an efflux transporter at the luminal mbrane of the brain capillaries in vivo, together with P-gp hinkel et al., 1994, 1996).

As a neurosteroid, dehydroepiandrosterone sulfate HEAS) and its unconjugated form (DHEA) modulates neuransmission in an excitatory or inhibitory manner via -gated channels involving *N*-methyl-D-aspartate receptors d γ-aminobutyric acid receptors (Schumacher et al., 1997). rodents, DHEAS and DHEA are also synthesized locally in brain, and these neurosteroids can be interchanged via fotransferase and sulfatase (Baulieu, 1996; Stoffel-Wagr, 2001), and the level of DHEAS is much higher than that DHEA in the brain and plasma of rats (Corpechot et al., 81). At least in rodents, a compartmental barrier is known exist for DHEAS between the brain and circulating blood iggio and Purdy, 2001), and in humans, the concentration DHEAS in brain is known to be much lower than that in ood (Weill-Engerer et al., 2002).

DHEAS is a substrate of several transporters, including a$^+$-taurocholate cotransporting polypeptides, organic an-transporting polypeptides (Oatp/OATP), and organic an- transporters (Oat/OAT) (Kullak-Ublick et al., 1998; agenbuch and Meier, 2003; Hasegawa et al., 2003). In parcular, Oatp2 (*Slco1a4*, OATP1a4) has been reported to be a ndidate efflux transporter for DHEAS at the BBB (Asaba al., 2000). Interestingly, Asaba et al. also suggested the xistence of primary active efflux transporter(s) for DHEAS a conditionally immortalized cell line established from ouse brain capillary endothelial cells (TM-BBB4). The net ptake of DHEAS by TM-BBB4 was increased under ATPepleted conditions (Asaba et al., 2000). This efflux transport ystem is expected to account for the compartmentalization f DHEAS between brain and the circulating blood and also o be one of the mechanisms of inactivation of DHEAS in the rain to regulate its activity on neurons.

Our previous study using membrane vesicles prepared rom BCRP overexpressed P-388 cells clearly showed that HEAS is an endogenous substrate of BCRP (Suzuki et al., 2003). Therefore, we hypothesized that BCRP plays a role in he luminal excretion of DHEAS at the brain capillaries as an nidentified primary active efflux transporter(s) predicted by Asaba et al. (2000). This hypothesis was partially supported by the results of Jonker et al. They showed that GF120918 (Elacridar), an acridine derivative known to be an inhibitor of P-gp and BCRP, increased the in vivo oral bioavailability and fetal penetration of topotecan even in Mdr1a/1b P-gp knockout mice, suggesting a function for BCRP in the intestinal barrier and maternal-fetal barrier (Jonker et al., 2000). In the present study, the expression and localization of Bcrp at the mouse BBB was investigated by real-time quantitative RT-PCR, Western blot analysis, and immunohistochemical staining. The brain uptake of DHEAS was determined using the in situ brain perfusion method, and the effect of GF120918 on brain uptake was examined. The brain uptake of mitoxantrone, a typical substrate of Bcrp, was also investigated in the same manner. Finally, the involvement of mouse Bcrp in the efflux of DHEAS and mitoxantrone across the BBB was evaluated directly using the recently established Bcrp knockout mouse (Jonker et al., 2002).

Materials and Methods

Reagents and Animals. [^{3}H]DHEAS was purchased from PerkinElmer Life and Analytical Sciences (Boston, MA). [^{14}C]Sucrose and [^{3}H]mitoxantrone were purchased from Moravek Biochemicals (Brea, CA). GF120918 was a gift from GlaxoSmithKline (Uxbridge, Middlesex, UK). USP grade propylene glycol was purchased from Sigma-Aldrich (St. Louis, MO). All other chemicals used in the experiments were of analytic grade.

Male Mdr1a/1b P-gp knockout mice and age-matched wild-type control mice were purchased from Taconic Farms (Germantown, NY), and male Bcrp knockout mice and age-matched wild-type mice of a comparable genetic background were produced as reported (Jonker et al., 2002). All mice (8 ~ 22 weeks) were maintained under standard conditions with a reverse dark/light cycle. Food and water were available ad libitum.

Isolation of Mouse Brain Capillaries. A brain capillary-enriched fraction from the mouse brain (BBB-enriched fraction) was isolated according to the reported procedure with slight modification (Dallaire et al., 1991; Ball et al., 2002). Briefly, large brains were dissected from the heads after perfusion with 0.9% saline and homogenized using a Polytron homogenizer in a 0.32 M sucrose solution and centrifuged at 4°C at 2200*g* for 10 min. The pellet was further purified according to the procedures suggested by Dallaire et al. (1991) and used as a BBB-enriched fraction. All reagents as well as the tissue should be kept on ice or as close to 4°C as possible throughout the isolation process to minimize degradation.

The purity of the isolated BBB-enriched fraction was checked by the enhanced alkaline phosphatase activity in the brain homogenate and BBB-enriched fraction (Dallaire et al., 1991; Ball et al., 2002). Isolated brain capillary-enriched fraction from mice contained tangled skeins of microvessel, which was confirmed under light microscopy. The alkaline phosphatase activity in the BBB-enriched fraction was 18.6-fold greater than that in the brain homogenate. This BBB-enriched fraction was used for further analyses: Western blot and real-time quantitative PCR.

Quantification of Transporter mRNA in the Brain Homogenate and the BBB-Enriched Fraction. To quantify the expression of Bcrp at the mouse BBB, real-time quantitative PCR was used. Total RNA was isolated from the BBB-enriched fraction and brain homogenate from wild-type FVB mice using an RNeasy mini kit (QIAGEN, Valencia, CA) and was converted to cDNA using random primer and avian myeloblastosis virus reverse transcriptase. Real-time quantitative PCR was performed using a QuantiTect SYBR Green PCR kit (QIAGEN) and LightCycler system (Roche Diagnostics, Mannheim, Germany) according to the manufacturer's instructions. The primers used in the quantification are listed in Table1. All primers were designed based on the published full sequence of each

TABLE 1
Nucleotide sequences of the primers used in quantitative PCR

	Forward Primer	Reverse Primer	Gene Bank Accession No.
HPRT	GCTTTCCCTGGTTAAGCAGTACA	CAAACTTGTCTGGAATTTCAAATC	J00423
Bcrp	AAATGGAGCACCTCAACCTG	CCCATCACAACGTCATCTTG	NM_011920
Mdr1a	TCATTGCGATAGCTGGAGTG	CAAACTTCTGCTCCCGAGTC	NM_011076
Mrp1	AGGCTGGAGCTAAGGAGGAG	CAGCCATGGAGTAGCCAAAT	NM_008576
Mrp4	GGTTGGAATTGTGGGCAGAA	TCGTCCGTGTGCTCATTGAA	XM_139262
Oatp2	ATAGCTTCAGGCGCATTTAC	TTCTCCATCATTCTGCATCG	NM_030687

protein. Hypoxanthine phosphoribosyl-transferase (HPRT) was used as a housekeeping gene for the internal standards, and Mdr1a was used as a positive control gene for putative transporter at the brain microvessel (Ball et al., 2002). An external standard curve was generated by dilution of the target PCR product, which was purified by agarose gel electrophoresis. The absolute concentration of external standard was measured by PicoGreen dsDNA Quantitation Reagent (Molecular Probes, Eugene, OR). To confirm amplification specificity, PCR products were subjected to a melting curve analysis and gel electrophoresis. All gene expressions in each reaction were normalized by the expression of HPRT in the same sample (Ball et al., 2002).

Besides Bcrp, the mRNA of Mdr1a, multidrug resistance-associated protein 1 (Mrp1), Mrp4, and Oatp2 in total brain cortex of wild-type and Bcrp knockout mouse were also measured by real-time quantitative PCR. These transporters have been reported to be expressed in the mouse brain, and this result was used to show the relative expression of these transporters in the wild-type mouse brain and to examine the possibility of up- and/or down-regulation of these transporters in the brain of the Bcrp knockout mouse.

Western Blot Analysis. The lysates of the BBB-enriched fraction and brain homogenate were subjected to electrophoresis on a 7.5% SDS-polyacrylamide gel. Proteins were transferred to nitrocellulose membranes (Immobilon; Millipore Corporation, Bedford, MA) which were blocked with Tris-buffered saline containing 0.05% Tween 20 (TBST) and 5% skim milk for 2 h at room temperature. After washing with TBST, membranes were incubated with anti-BCRP monoclonal antibody (40-fold diluted BXP-53 antibody; Signet Laboratories, Dedham, MA) in TBST overnight at 4°C, and proteins were detected using the ECL system (Amersham Biosciences Inc., Arlington Heights, IL).

Immunocytochemical Analysis of the Expression of Bcrp at the Mouse BBB. Brain samples from the wild-type mouse and Bcrp knockout mouse were fixed in 4% phosphate-buffered formalin, embedded in paraffin, sectioned at 4 μm, and stained with hematoxylin and eosin according to standard procedures. For immunohistochemistry, tissues were deparaffinized in xylene and rehydrated. Endogenous peroxidase activity was blocked by 3% (v/v) H_2O_2 in methanol for 10 min. Before staining, paraffin sections were pretreated by heat-induced epitope retrieval. Slides were incubated with 5% normal goat serum/PBS for 30 min, and subsequently, sections were incubated overnight with a 1:400 dilution of BXP-53 at 4°C. Monoclonal antibody immunoreactivity was detected by the streptavidin-biotin immunoperoxidase (sABC) method by using biotinylated goat anti-rat IgG (Dako, 1:100) as a secondary antibody and diaminobenzidine substrate for visualization. After counterstaining with hematoxylin, slides were mounted. To investigate the localization of Bcrp in brain microvessels, double immunostaining with antibodies of P-gp (luminal expression) and glucose transporter 1 (Glut1, luminal and abluminal coexpression) was also performed using cryostat sections of wild-type mouse brain (10-μm thick) (Cooray et al., 2002). Brain sections without fixation were incubated overnight at 4°C with primary antibody at the following concentrations: Bxp-53 (Bcrp, 1:40 dilution in 1% BSA/PBS), C219 (P-gp, 1:40 dilution in 1% BSA/PBS; Signet Laboratories), and anti-Glit1 (Glut1, 1:40 dilution in 1% BSA/PBS; Santa Cruz Biochemicals, Santa Cruz, CA). After washing with PBS, sections were incubated with appropriate Alexa Fluor secondary antibodies (Molecular Probes) and Topro3 (DNA dye; Molecular Probes, Hilversum, Netherlands) for 1 h and mounted in Vectashield mounting medium (Vector Laboratories, Burlingame, CA) and visualized under a Zeiss confocal fluorescence microscope.

In Situ Brain Perfusion to Determine the Brain Uptake of Bcrp Substrates. The right cerebral hemisphere of the mouse was perfused using the reported method (Takasato et al., 1984, Dagenais et al., 2000; Murakami et al., 2000) with minor modification. In brief, the mouse was anesthetized by intraperitoneal injection of 10 mg/kg xylazine (Sigma-Aldrich) and 100 mg/kg ketamine (Sankyo Co., Tokyo, Japan). The right common carotid artery was exposed and then catheterized with polyethylene tubing (0.2 mm i.d. × 0.5 mm o.d; Natsume, Tokyo, Japan) filled with heparinized saline. The right hemisphere of the brain was perfused with Krebs bicarbonate buffer (pH 7.4 with 95% O_2 and 5% CO_2 containing 10 mM D-glucose) at a flow rate of 1 ml/min (Murakami et al., 2000). The thorax of the mouse was opened, and the cardiac ventricle was severed immediately before perfusion. [^{3}H]DHEAS or [^{3}H]mitoxantrone was added to perfusate at a concentration of 1 μCi/ml with carbon-labeled sucrose as a vascular volume marker. Perfusion was terminated by decapitation at selected times (1 and 2 min, for [^{3}H]DHEAS; 1.5 min for [^{3}H]mitoxantrone). The right hemisphere of the brain was removed from the skull and weighed. Aliquots of the perfusion fluid also were collected to determine tracer concentrations in the perfusate. Brain samples were digested in 2 ml 1 N NaOH at 55°C, and the dual radioactivity associated with the brain was measured in a liquid scintillation counter (LS 6000SE; Beckman Coulter, Fullerton, CA).

In all perfusion experiments, the brain vascular volume (V_{vasc}; microliter per gram) was estimated from the tissue distribution of [^{14}C]sucrose, which is known to diffuse very slowly across the BBB, using the following equation (Dagenais et al., 2000):

$$V_{vasc} = X_{sucrose}/C_{sucrose} \quad (1)$$

where $X_{sucrose}$ (disintegrations per minute per gram) is the amount of sucrose measured in the right brain hemisphere and $C_{sucrose}$ (disintegrations per minute per milliliter) is the concentration of labeled sucrose in the perfusion fluid. V_{vasc} is the brain vascular distribution volume of substrate used to check BBB integrity during the experiments (Dagenais et al., 2000).

Brain distributional volume of substrate (V_{brain}, microliters per gram) is calculated as:

$$V_{brain} = X_{brain}/C_{substrate} \quad (2)$$

where X_{brain} is the amount of substrate in the brain (disintegrations per minute per gram) corrected for vascular contamination ($X_{total} - V_{vasc} \times C_{substrate}$) and $C_{substrate}$ is the concentration of substrate in the perfusate (disintegrations per minute per milliliter) (Dagenais et al., 2000).

The uptake clearance of substrate (CL_{up}, microliters per gram) is calculated as the slope of the plot of time versus V_{brain}.

$$CL_{up} = X_{brain}/T/C_{substrate} \quad (3)$$

where T is the perfusion time (min) (Dagenais et al., 2000).

Effects of Bcrp and P-gp on the Brain Uptake of [^{3}H]DHEAS and [^{3}H]Mitoxantrone. As an inhibitor of Bcrp, GF120918 (10 or 20 mg/kg, dissolved in a 3:2 mixture of propylene glycol/water) was injected intravenously to mice (125 μl/25g mice) at 10 min before the in situ perfusion of [^{3}H]DHEAS and [^{3}H]mitoxantrone (Hyafil et al., 1993, Cisternino et al., 2001). Because GF120918 inhibits both P-gp and Bcrp (Allen et al., 1999), the role of Bcrp on the brain uptake of substrates was investigated by comparing the brain uptake in wild-type control mice and P-pg knockout mice with or without treatment with GF120918, respectively, to exclude any confounding effects of P-gp inhibition (Jonker et al., 2000). The role of Bcrp on BBB transport was also examined directly by comparing the brain uptake of [^{3}H]DHEAS and [^{3}H]mitoxantrone in Bcrp knockout mice and wild-type control mice (Jonker et al., 2002). Control groups received only vehicle solution in all experiments.

Statistical Analysis. Data are presented as the mean ± standard error for 3 to 10 animals unless specified otherwise. Student's two-tailed unpaired t test and one-way ANOVA followed by the Newman-Keuls multiple comparison test were used to identify significant differences between groups when appropriate. Statistical significance was set at $p < 0.05$.

Results

The Expression of Bcrp at the Mouse BBB. The expression of Bcrp at the BBB was suggested by comparing

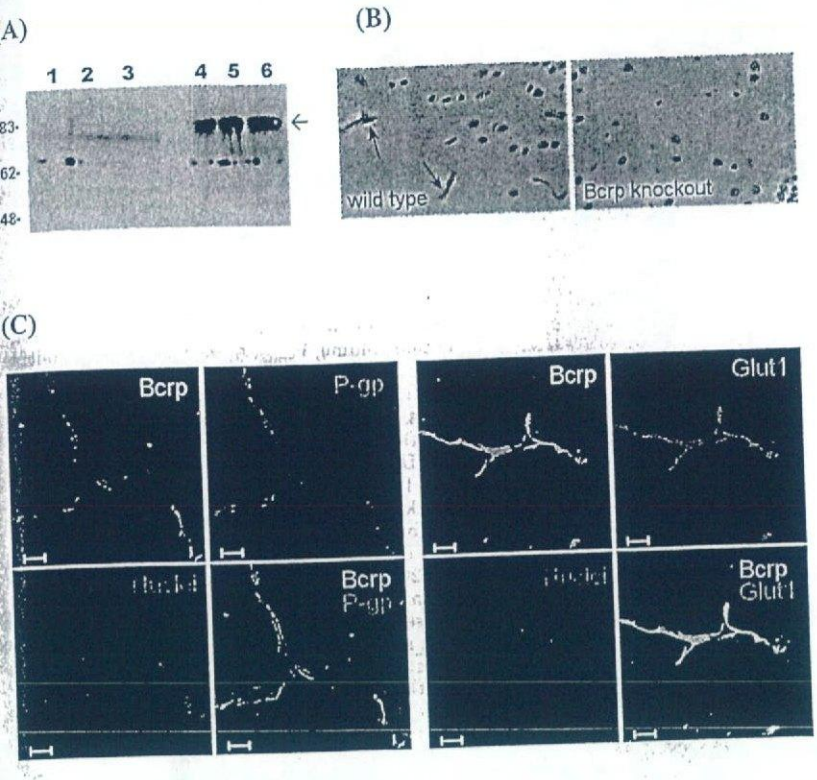

Fig. 1. Expression of Bcrp at the BBB. A, Western blot of brain homogenate and the BBB-enriched fraction with anti-mouse BCRP monoclonal antibody (BXP-53). Approximately 70 kDa of Bcrp band in BBB-enriched fraction was clearly detected (lanes 4–6), whereas only faint bands were observed in brain (lanes 1–3). Lane 1, 4 (25 μg of protein); lane 2, 5 (50 μg of protein); lane 3, 6 (100 μg of protein). B, immunohistochemical detection of Bcrp in brain sections from wild-type (left) and Bcrp knockout mice (right). A consistent staining of blood capillaries for Bcrp (brown) throughout the mouse brain was observed, suggesting moderate Bcrp expression in wild-type brain capillaries, whereas it was completely absent in the Bcrp knockout mouse brain. C, double immunostaining of Bcrp with P-gp and Glut1. P-gp was used as a marker of luminal expression and Glut1 was used as a marker of luminal and abluminal coexpression: green, Bcrp; red, P-gp (left) or Glut1 (right); blue color indicates nuclei stained with Topro3. The Bcrp and P-gp signals were completely superimposed, whereas the Bcrp signal only partially overlapped with Glut1 signals, suggesting luminal expression of Bcrp in brain capillaries. Scale bar = 10 μm.

mRNA expression between brain homogenate and capillary-enriched fraction by real-time quantitative PCR. The concentration of Bcrp mRNA, which was normalized by that of HPRT, was 5.6-fold higher in the BBB-enriched fraction than that in brain homogenate (5.6 ± 1.3, mean ± S.D.), whereas that of Mdr1a mRNA was enriched 12-fold in the BBB-enriched fraction (12 ± 2, mean ± S.D.).

The protein band (70 kDa) of Bcrp in the BBB-enriched fraction was clearly detected by Western blot analysis using monoclonal antibody BXP-53, whereas only weak staining was observed in the brain homogenate, suggesting that the primary localization of Bcrp is at the BBB (Fig. 1A). Furthermore, immunohistochemical analysis of brain sections of wild-type and Bcrp knockout mice showed Bcrp expression only in the brain capillaries of the wild-type mouse (Fig. 1B). Although the absolute staining level does not appear to be very high, Bcrp-related staining of blood capillaries throughout the mouse brain was clearly observed, whereas it was completely absent in Bcrp knockout mouse brain (Fig. 1B). Double immunostaining of Bcrp with P-gp and Glut1 clearly showed that Bcrp is expressed at the luminal side of brain microvessels (Fig. 1C). The Bcrp signal was completely superimposed on that of P-gp expressed at the luminal side of the brain microvessels. However, the Bcrp signal only partially overlapped with that of Glut1 expressed at the abluminal and luminal side of the brain microvessel.

The Effect of Pretreatment with GF120918 on the Brain Uptake of [^{3}H]DHEAS and [^{3}H]Mitoxantrone. The time-dependent brain uptake of [^{3}H]DHEAS in mice is shown in Fig. 2. The brain uptake increased linearly, and the uptake clearances could be calculated from the slope of the plot of V_{brain} versus time (Dagenais et al., 2000). The brain uptake clearance of [^{3}H]DHEAS was 18.0 μl/min/g of brain (Fig. 2). Pretreatment of wild-type mice with GF120918 (10 mg/kg) increased the brain uptake clearance of [^{3}H]DHEAS about 2.1-fold (approximately estimated, 38.6 μl/min/g of brain). Increasing the dose of GF120918 (20 mg/kg) showed a further increase in the brain uptake of [^{3}H]DHEAS by 3.0-fold (approximately estimated, 54.0 μl/min/g of brain) (Fig. 2). The V_{brain} of [^{3}H]DHEAS at 2 min was increased 2.0- and 2.8-fold by pretreatment with GF120918 10 and 20 mg/kg, respectively (Fig. 2; *, $p < 0.05$).

The brain uptake of [^{3}H]DHEAS (Fig. 3A) in Mdr1a/1b P-gp knockout mice was comparable with that in wild-type mice. However, GF120918 (10 mg/kg) increased the brain uptake of [^{3}H]DHEAS even in the Mdr1a/1b P-gp knockout

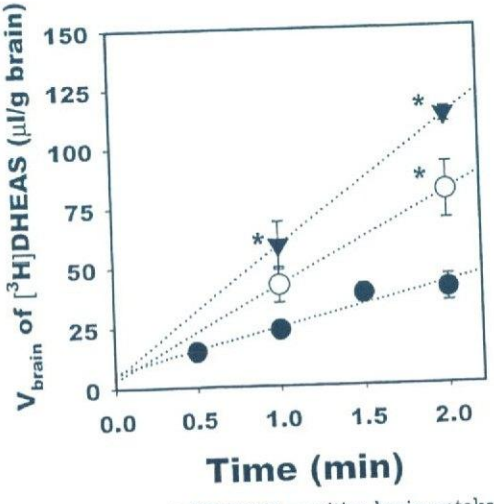

Fig. 2. Time-dependent and GF120918-sensitive brain uptake of [^{3}H]DHEAS. Brain uptake is expressed as brain distribution volume, V_{brain} and uptake clearances could be calculated by the slope of plot of V_{brain} versus time profile. ●, control, CL_{up} = 18.0 μl/min/g of brain; ○, +GF120918, 10 mg/kg, CL_{up} = 38.6 μl/min/g of brain; ▼, +GF120918, 20 mg/kg, CL_{up} = 54.0 μl/min/g of brain (n = 3 ~ 10 per point; *, statistically different with control, $p < 0.05$).

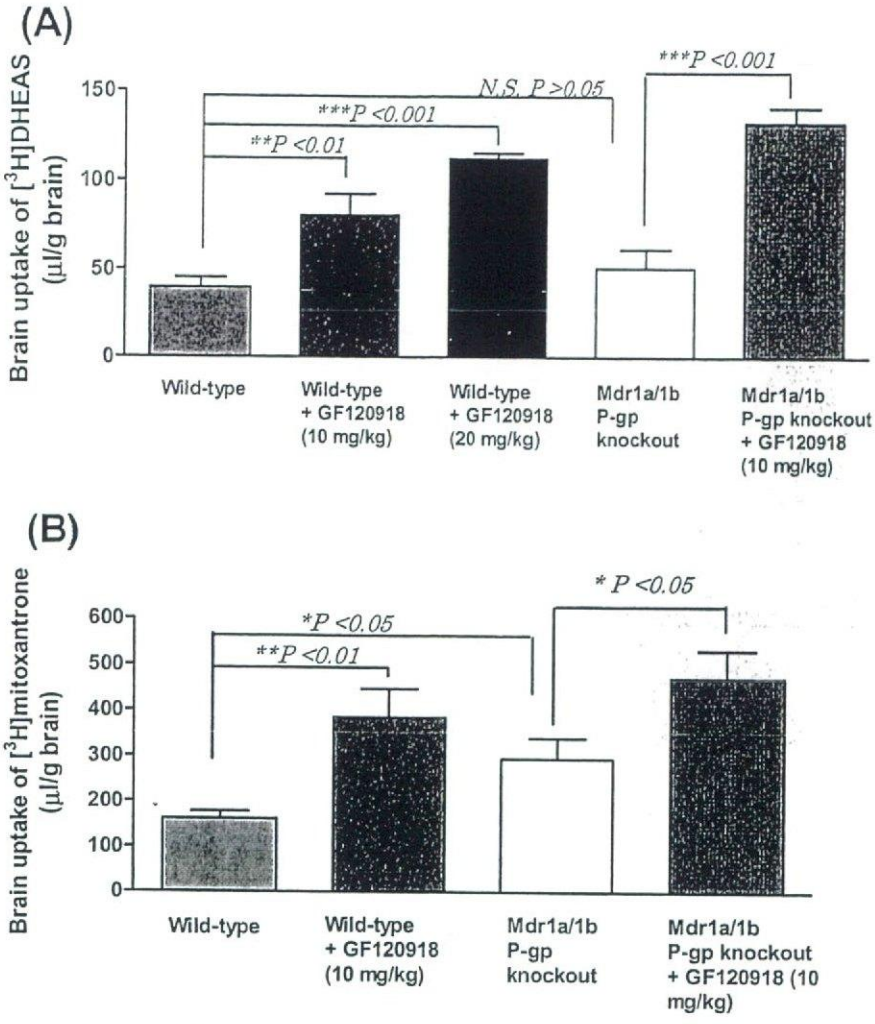

Fig. 3. Brain uptake of [^{3}H]DHEAS and [^{3}H]mitoxantrone, which was expressed as brain distribution volume, V_{brain}. A, the GF120918-sensitive brain uptake of [^{3}H]DHEAS at 2 min after in situ brain perfusion (V_{brain} at 2 min). The pretreatment of GF120918 increased the brain uptake of [^{3}H]DHEAS, whereas knockout of Mdr1a/1b did not. Data are presented as the mean ± S.E. (n = 3 ~ 10 per point). B, GF120918-sensitive brain uptake of [^{3}H]mitoxantrone at 1.5 min after in situ brain perfusion (V_{brain} at 1.5 min). A knockout of Mdr1a/1b and the pretreatment of GF120918 increased the brain uptake of [^{3}H]mitoxantrone. The pretreatment of GF120918 increased the brain uptake of [^{3}H]mitoxantrone even in Mdr1a/1b P-gp knockout mice. Data are presented as the mean ± S.E. (n = 4 ~ 6 per point). Statistical significance was calculated by one-way ANOVA followed by Newman-Keuls multiple comparison tests.

mice (Fig. 3A). The V_{brain} of [^{3}H]DHEAS at 2 min was increased 2.6-fold by pretreatment with GF120918 (10 mg/kg) in Mdr1a/1b P-gp knockout mice compared with that in the nontreated group.

The brain uptake of [^{3}H]mitoxantrone in wild-type mice and Mdr1a/1b P-gp knockout mice, with or without pretreatment with GF120918, is presented in Fig. 3B. The brain uptake of [^{3}H]mitoxantrone was increased in Mdr1a/1b P-gp knockout mice (1.8-fold) and wild-type mice following pretreatment with GF120918 (10 mg/kg, 2.4-fold). GF120918 (10 mg/kg) also increased the brain uptake of [^{3}H]mitoxantrone in Mdr1a/1b P-gp knockout mice (1.6-fold). The inhibitory effect of GF120918 was found to be more potent in Mdr1a/1b P-gp knockout mice for [^{3}H]DHEAS (Fig. 3A, wild-type + GF120918, 10 mg versus Mdr1a/1b P-gp knockout + GF120918, 10 mg; $p < 0.05$ Newman-Keuls multiple comparison test), although the reason was unclear. In the case of [^{3}H]mitoxantrone, no significant difference was noted between the wild-type + GF120918 10-mg group and the Mdr1a/1b P-gp knockout + GF120918 10-mg group.

Effect of Bcrp Gene Knockout on the Brain Uptake of [^{3}H]DHEAS and [^{3}H]Mitoxantrone. The impact of Bcrp on the transport of [^{3}H]DHEAS and [^{3}H]mitoxantrone across the BBB was evaluated directly using the Bcrp gene knockout mouse (Fig. 4, A and B). The brain uptake of [^{3}H]DHEAS in Bcrp knockout mice was not different from that in wild-type mice (Fig. 4A). Pretreatment with GF120918 (10 mg/kg) increased the brain uptake of [^{3}H]DHEAS even in Bcrp knockout mice. The V_{brain} of [^{3}H]DHEAS at 2 min was increased about 1.8- and 2.2-fold by GF120918 (10 mg/kg) in wild-type and Bcrp knockout mice, respectively.

In addition, the brain uptake of [^{3}H]mitoxantrone in Bcrp knockout mice was no different from that in wild-type mice (Fig. 4B). The V_{brain} of [^{3}H]mitoxantrone at 1.5 min was 144 ± 3 μl/g brain (n = 3) in the wild-type mouse and 161 ± 18 μl/g brain (n = 3) in the Bcrp knockout mouse, respectively, and there was no statistical difference between the two groups (unpaired Student's t test, $p > 0.05$).

Assessment of BBB Integrity. In all experiments, the physical integrity of the BBB was assessed by [^{14}C]sucrose, which serves as a brain vascular space marker. The brain vascular space under each set of experiment conditions was not changed by knockout of the Mdr1a/1b gene and pretreatment with GF120918 (Table 2). A similar brain vascular space was also observed between Bcrp knockout mice and their wild-type controls suggesting that the BBB integrity was not adversely affected by these experiments.

Relative Expression of Transporters in Mouse Brain. To estimate the relative expression of these transporters in the wild-type mouse brain and to examine the possibility of up- and/or down-regulation of these transporters in the brain of the Bcrp knockout mouse, mRNA quantification of known transporters such as Mdr1a, Mrp1, Mrp4, and Oatp2 was carried out using cDNA prepared from mouse brain homog-

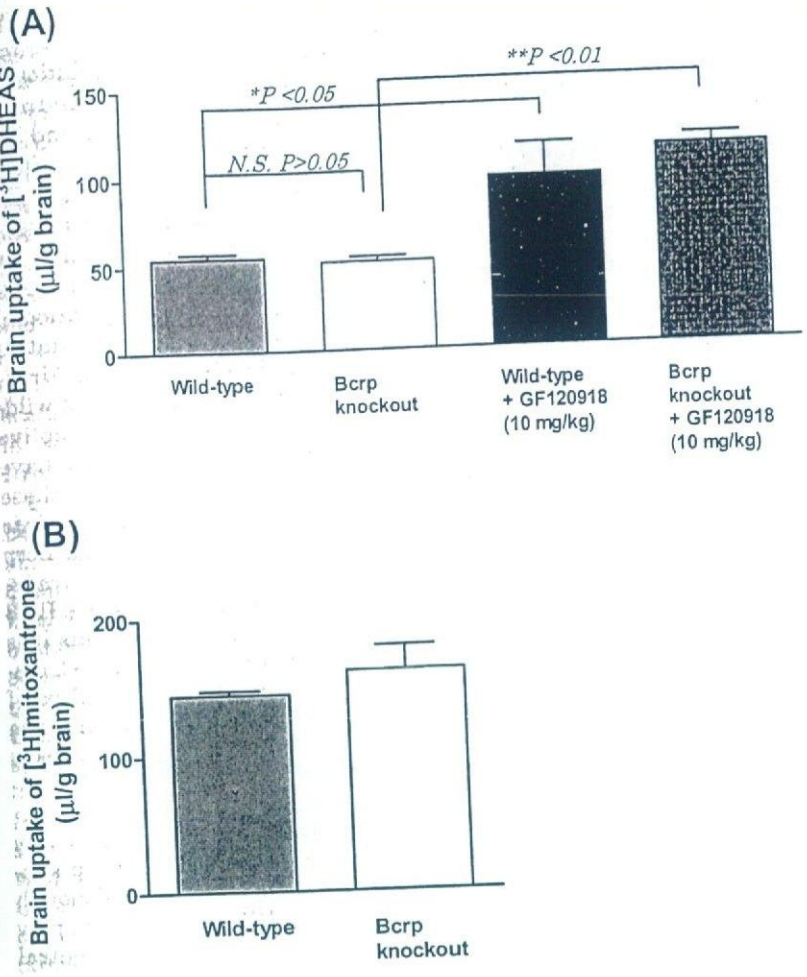

Fig. 4. Brain uptake of [^{3}H]DHEAS and [^{3}H]mitoxantrone in Bcrp knockout mice. A, the brain uptake of [^{3}H]DHEAS in Bcrp knockout mice was not different with that in wild-type control mice of the same genetic background, and the brain uptake of [^{3}H]DHEAS was increased by treatment of GF120918 in wild-type mice and even in Bcrp knockout mice. Data are presented as the mean ± S.E. (n = 3, respectively). Statistical significance was calculated by one-way ANOVA followed by Newman-Keuls multiple comparison tests. B, brain uptake of [^{3}H]mitoxantrone. The brain uptake of [^{3}H]mitoxantrone in Bcrp knockout mice was not different with that in wild-type control mice. Data are presented as the mean ± S.E. (n = 3, respectively). Statistical significance was calculated by unpaired t test.

TABLE 2

Vascular volume (V_{vasc}, microliters per gram of brain) of mouse brain in each experiment

Vascular volume was determined by coperfusion of [^{14}C]sucrose for 2 min ([^{3}H]DHEAS) or 1.5 min ([^{3}H]mitoxantrone). Vascular volumes did not differ significantly between any of the experiments ($p > 0.05$, one-way ANOVA). Data are presented as the mean ± S.E. (n = 4 ~ 10 per point).

Vascular Volume	Wild-Type Mice			Mdr1a/1b P-gp Knockout Mice		Bcrp Knockout Mice	
	Control	GF120918		Control	GF120918 (10 mg/kg)	Control	GF120918 (10 mg/kg)
		10 mg/kg	20 mg/kg				
μl/g brain							
DHEAS	12.8 ± 1.2	16.9 ± 1.9	15.5 ± 0.8	11.3 ± 0.8	12.4 ± 0.5	11.3 ± 0.5	8.96 ± 1.26
Mitoxantrone	11.9 ± 2.6	11.3 ± 4.3		16.6 ± 1.8	16.7 ± 4.3	12.9 ± 1.3	13.0 ± 1.6

enate (Table 3). Each value represents the mRNA level in the brain homogenate from one single mouse normalized by the mRNA level of HPRT in the same sample. Except for Oatp2, mRNA levels of other transporters in wild-type mouse brain were comparable ($p > 0.05$, one-way ANOVA followed by the Newman-Keuls multiple comparison test). The mRNA levels of Oatp2 were statistically different with those of other transporters ($p < 0.05$, one-way ANOVA followed by the Newman-Keuls multiple comparison test). The mRNA levels of all transporters in the brain of the Bcrp knockout mouse were similar to those in the brain of the wild-type mouse, except for the case of Bcrp. It is interesting that Mrp4 shows abundant expression in the brain homogenate, as much as Mdr1a. Furthermore, the concentration of Mrp4 mRNA was 4.7-fold greater in the BBB-enriched fraction than in the brain homogenate.

TABLE 3

The expression of Bcrp, Mdr1a, Mrp1, Mrp4, and Oatp2 in brain homogenate

All mRNA levels were measured by real-time quantitative PCR and normalized by the concentration of HPRT. These were results from independent cDNA samples from three wild-type and Bcrp knockout mice, respectively (n = 3 ~ 4, mean ± S.D., ratio to HRPT). BCRP KO and ND represent Bcrp knockout mice and not detected, respectively.

	Bcrp	Mdr1a	Mrp1	Mrp4	Oatp2
Wild-type	18.1 ± 2.3	26.9 ± 5.9	17.4 ± 1.1	27.7 ± 2.2	40.8 ± 7.6
Bcrp KO	ND	28.4 ± 3.3	19.1 ± 7.6	26.9 ± 1.9	44.2 ± 7.2

Discussion

In the present study, we examined the involvement of Bcrp in the efflux transport of DHEAS using the in situ brain perfusion method to examine the hypothesis that BCRP acts as a functional efflux transporter at the BBB for sulfoconjugated organic anions. In addition, the role of BCRP at the BBB was also investigated using another typical BCRP substrate, mitoxantrone.

Quantitative real-time PCR showed that the concentration of Bcrp mRNA in the brain was comparable with that of ABC transporters which are expressed in the mouse brain, such as Mdr1a, Mrp1, and Mrp4 (Table 3) and that Bcrp mRNA was enriched in the BBB-enriched fraction similar to Mdr1a P-gp mRNA. Western blot analysis revealed that Bcrp was clearly detectable in the BBB-enriched fraction, and the band density was greater in the BBB-enriched fraction than in the brain homogenate (Fig. 1A). Furthermore, immunohistochemical analysis revealed that Bcrp was localized at the luminal side of mouse brain capillaries (Fig. 1, B and C). All these results indicate that Bcrp is expressed and localized at the BBB, suggesting the possibility the Bcrp may play a role in the efflux of its substrates at the BBB.

Involvement of Bcrp in the transport of DHEAS and mitoxantrone at the BBB was investigated by examining the effect of GF120918 on their brain uptake determined using the in situ brain perfusion technique in the mouse. Because GF120918 inhibits both P-gp and Bcrp (Allen et al., 1999), the P-pg knockout mouse was used in conjunction with the wild-type mouse to exclude any confounding effects of P-gp inhibition (Jonker et al., 2000). Time-dependent brain uptake of [^{3}H]DHEAS was observed up to 2 min, and treatment with GF120918 increased the brain uptake of [^{3}H]DHEAS in a dose-dependent manner (Fig. 2), whereas it did not affect the distribution volume of sucrose (Table 2). This suggests that the effect of GF120918 is not due to a nonspecific effect, such as the destruction of the BBB by opening the tight junctions, but to inhibition of efflux transport at the BBB. Since GF120918 is an inhibitor of both P-gp and Bcrp (Allen et al., 1999), the brain uptake of [^{3}H]DHEAS was also determined in the Mdr1a/1b P-gp knockout mouse to exclude the possibility that the effect of GF120918 is due to inhibition of P-gp at the BBB (Fig. 3A). The brain uptake of [^{3}H]DHEAS in Mdr1a/1b P-gp knockout mice was comparable with that in wild-type mice, and the increased brain uptake of [^{3}H]DHEAS by GF120918 was still observed in Mdr1a/1b P-gp knockout mice (Fig. 3A). In the case of another typical substrate of Bcrp, mitoxantrone, GF120918 treatment increased the brain uptake of [^{3}H]mitoxantrone similar to that of [^{3}H]DHEAS (Fig. 3B). Since the brain uptake of [^{3}H]mitoxantrone was increased in Mdr1a/1b P-gp knockout mice compared with that in wild-type mice (Fig. 3B), the effect of GF120918 is partly accounted for by inhibition of P-gp. However, GF120918 was still effective in wild-type and Mdr1a/1b P-gp knockout mice (Fig. 3B). Therefore, in addition to P-gp, it is likely that a GF120918-sensitive transporter other than P-gp is involved in the efflux of mitoxantrone at the BBB. Recently, Cisternino et al. (2004) also reported that the brain uptake of mitoxantrone was linear up to 2 min using the in situ perfusion method, and its uptake was increased by treatment of GF120918. This is consistent with our results; although, there is a discrepancy in the effect of knockout of P-gp on the brain uptake of [^{3}H]mitoxantrone for some, as yet unknown, reason (Cisternino et al., 2004).

To show that the effect of GF120918 is due to inhibition of Bcrp, the brain uptake of [^{3}H]DHEAS and [^{3}H]mitoxantrone was determined in Bcrp knockout mice (Fig. 4, A and B). Surprisingly, the brain uptake of [^{3}H]DHEAS and [^{3}H]mitoxantrone was found to be comparable and independent of the Bcrp expression (Fig. 4, A and B). Furthermore, treatment with GF120918 still increased the brain uptake of [^{3}H]DHEAS even in Bcrp knockout mice (Fig. 4A). To examine the possibility of adaptive up- and/or down-regulation of transporters in the brain of Bcrp knockout mice, quantitative PCR was carried out. The mRNA levels of Mdr1a, Mrp1, Mrp4, and Oatp2 were similar to those in the brain of wild-type mice (Table 3). This suggests that distinct adaptive alteration of the expression of transporters may not have occurred in the brain of Bcrp knockout mice as far as these transporters are concerned. Taking all these results into consideration, especially the in situ analysis using Bcrp knockout mice, the contribution of Bcrp to the efflux transport of [^{3}H]DHEAS and [^{3}H]mitoxantrone at the mouse BBB was considered to be minor, if it exists at all, and thus it is suggested that other GF120918-sensitive transporter(s), distinct from Bcrp and P-gp, may account for the efflux of [^{3}H]DHEAS and [^{3}H]mitoxantrone at the BBB. Whether one and the same GF120918-sensitive efflux transporter affects [^{3}H]DHEAS and [^{3}H]mitoxantrone remains to be demonstrated.

Collectively, the present study could not demonstrate any involvement of Bcrp in the efflux transport of the Bcrp substrates, DHEAS and mitoxantrone, at the BBB, although Bcrp is abundantly expressed at the BBB and is likely to play an important role as a detoxification system in the central nervous system together with P-gp. This result is also supported by the recent findings of van Herwaarden et al. (2003). They reported that the hepatobiliary and intestinal elimination of 2-amino-1-methyl-6-phenylimidazo[4,5-*b*]pyridine was significantly reduced in Bcrp knockout mice; however, there was no significant change in the brain penetration between wild-type and Bcrp knockout mice. The functional role of Bcrp at the BBB remains virtually unknown. Mogi et al. (2003) reported that Akt signaling modulates the side population cell phenotype by regulating the translocation of Bcrp between the plasma membrane and intracellular compartment. We cannot exclude the possibility that the function of Bcrp at the BBB is also modulated by an unknown mechanism and works only under certain conditions. Further investigation is necessary to elucidate the role of Bcrp in the detoxification system in the brain. Cisternino et al. (2004) also demonstrated that the brain uptake of prazosin and mitoxantrone was increased by treatment with GF120918 in Mdr1a single knockout mice. It would be interesting to discover whether the effect of GF120918 on the brain uptake of prazosin is also ascribed to the inhibition of Bcrp-mediated efflux.

The present study shows the presence of a GF120918-sensitive efflux transporter for [^{3}H]DHEAS and [^{3}H]mitoxantrone at the BBB. The uptake transporter, Oatp2, is expressed in the luminal and abluminal membrane of the brain capillaries. According to the in situ study by Dagenais et al. (2001), the brain uptake of [D-penicillamine(2,5)]-enkephaline, a peptide substrate of Oatp2 in Mdr1a P-gp knockout

nice was saturable and inhibited by Oatp2 substrates, suggesting the involvement of Oatp2. Therefore, it is possible that Oatp2 accounts for the luminal uptake of DHEAS at the luminal membrane of brain capillaries as well as efflux from the brain at the abluminal membrane. Although the physiological meaning of luminal Oatp2 remains unknown, this uptake is also considered to be present in humans since the human isoform of Oatp2, OATP-A, has been shown to exhibit similar membrane localization in the brain capillaries (Gao et al., 1999, 2000). Thus, it may be important to limit Oatp2- and OATP-A-mediated DHEAS uptake by the GF120918-sensitive efflux transporter at the BBB in addition to facilitate the elimination of locally synthesized DHEAS from the brain to regulate the effect of DHEAS on neuronal function. In addition, the efflux transporter may account for the DHEAS compartmentalization between the brain and blood.

Currently no candidate transporter other than P-gp and Bcrp has been reported to interact with GF120918 (Hyafil et al., 1993; Allen et al., 1999; Evers et al., 2000). Interestingly, quantification of mRNA revealed the abundant expression of MRP4 (*ABCC4*), an ABC transporter classified as a member of the Mrp/MRP (*ABCC*) family, in the brain compared with other ABC transporters such as P-gp and Mrp1. Furthermore, Mrp4 mRNA was increased in the BBB-enriched fraction like Mdr1a and Bcrp. RT-PCR analyses have demonstrated its expression in primary cultured bovine brain capillary endothelial cells and the brain capillary-enriched fraction (Zhang et al., 2000). MRP4 shows broad substrate specificity for a number of compounds including DHEAS as well as cyclic nucleotides, methotrexate, estradiol-17β-glucuronide, and prostaglandins (van Aubel et al., 2002; Zelcer et al., 2003). In the revision process of this article, Leggas et al. (2004) reported that Mrp4 is localized at the luminal membrane of the brain capillaries and decreased the efflux rate of topotecan from the brain in Mrp4 knockout mice compared with wild-type mice. These recent results may support our speculation, and further investigation is necessary to show that Mrp4 is also involved in the efflux transport of organic anions at the BBB.

In conclusion, we have demonstrated that a GF120918-sensitive transporter(s) is involved in the efflux of [^{3}H]DHEAS and [^{3}H]mitoxantrone at the BBB, facilitating their elimination from the brain and limiting their uptake by the brain. Although BCRP is abundantly expressed in blood capillaries forming the BBB, we did not find any evidence indicating that Bcrp is a functionally active efflux transporter at the BBB.

Acknowledgments

We thank Dr. Glynis Nicholls and GlaxoSmithKline Research and Development for help during this work and for the kind gift of GF120918.

References

Allen JD, Brinkhuis RF, Wijnholds J, and Schinkel AH (1999) The mouse Bcrp1/Mxr/Abcp gene: amplification and overexpression in cell lines selected for resistance to topotecan, mitoxantrone, or doxorubicin. *Cancer Res* 59:4237–4241.

Asaba H, Hosoya K, Takanaga H, Ohtsuki S, Tamura E, Takizawa T, and Terasaki T (2000) Blood-brain barrier is involved in the efflux transport of a neuroactive steroid, dehydroepiandrosterone sulfate, via organic anion transporting polypeptide 2. *J Neurochem* 75:1907–1916.

Ball HJ, McParland B, Driussi C, and Hunt NH (2002) Isolating vessels from the mouse brain for gene expression analysis using laser capture microdissection. *Brain Res Brain Res Protoc* 9:206–213.

Baulieu EE (1996) Dehydroepiandrosterone (DHEA): a fountain of youth? *J Clin Endocrinol Metab* 81:3147–3151.

Biggio G and Purdy RH (2001) Neurosteroids and brain function, in *International Review of Neurobiology* (Bradley RJ, Harris RA, and Jenner P eds) vol 46, pp 1–32, Academic Press, San Diego.

Cisternino S, Mercier C, Bourasset F, Roux F, and Scherrmann JM (2004) Expression, up-regulation and transport activity of the multidrug-resistance protein Abcg2 at the mouse blood-brain barrier. *Cancer Res* 64:3296–3301.

Cisternino S, Rousselle C, Dagenais C, and Scherrmann JM (2001) Screening of multidrug-resistance sensitive drugs by in situ brain perfusion in P-glycoprotein-deficient mice. *Pharm Res (NY)* 18:183–190.

Cooray HC, Blackmore CG, Maskell L, and Barrand MA (2002) Localisation of breast cancer resistance protein in microvessel endothelium of human brain. *Neuroreport* 13:2059–2063.

Corpechot C, Robel P, Axelson M, Sjovall J, and Baulieu EE (1981) Characterization and measurement of dehydroepiandrosterone sulfate in rat brain. *Proc Natl Acad Sci USA* 78:4704–4707.

Dagenais C, Ducharme J, and Pollack GM (2001) Uptake and efflux of the peptidic delta-opioid receptor agonist [D-penicillamine2,5]-enkephalin at the murine blood-brain barrier by in situ perfusion. *Neurosci Lett* 301:155–158.

Dagenais C, Rousselle C, Pollack GM, and Scherrmann JM (2000) Development of an in situ mouse brain perfusion model and its application to mdr1a P-glycoprotein-deficient mice. *J Cereb Blood Flow Metab* 20:381–386.

Dallaire L, Tremblay L, and Beliveau R (1991) Purification and characterization of metabolically active capillaries of the blood-brain barrier. *Biochem J* 276:745–752.

Eisenblatter T and Galla HJ (2002) A new multidrug resistance protein at the blood-brain barrier. *Biochem Biophys Res Commun* 293:1273–1278.

Evers R, Kool M, Smith AJ, van Deemter L, de Haas M, and Borst P (2000) Inhibitory effect of the reversal agents V-104, GF120918 and Pluronic L61 on MDR1 Pgp-, MRP1- and MRP2-mediated transport. *Br J Cancer* 83:366–374.

Gao B, Hagenbuch B, Kullak-Ublick GA, Benke D, Aguzzi A, and Meier PJ (2000) Organic anion-transporting polypeptides mediate transport of opioid peptides across blood-brain barrier. *J Pharmacol Exp Ther* 294:73–79.

Gao B, Stieger B, Noe B, Fritschy JM, and Meier PJ (1999) Localization of the organic anion transporting polypeptide 2 (Oatp2) in capillary endothelium and choroid plexus epithelium of rat brain. *J Histochem Cytochem* 47:1255–1264.

Hagenbuch B and Meier PJ (2003) The superfamily of organic anion transporting polypeptides. *Biochim Biophys Acta* 1609:1–18.

Hasegawa M, Kusuhara H, Endou H, and Sugiyama Y (2003) Contribution of organic anion transporters to the renal uptake of anionic compounds and nucleoside derivatives in rat. *J Pharmacol Exp Ther* 305:1087–1097.

Hyafil F, Vergely C, Du Vignaud P, and Grand-Perret T (1993) In vitro and in vivo reversal of multidrug resistance by GF120918, an acridonecarboxamide derivative. *Cancer Res* 53:4595–4602.

Jonker JW, Buitelaar M, Wagenaar E, Van Der Valk MA, Scheffer GL, Scheper RJ, Plosch T, Kuipers F, Elferink RP, Rosing H, et al. (2002) The breast cancer resistance protein protects against a major chlorophyll-derived dietary phototoxin and protoporphyria. *Proc Natl Acad Sci USA* 99:15649–15654.

Jonker JW, Smit JW, Brinkhuis RF, Maliepaard M, Beijnen JH, Schellens JH, and Schinkel AH (2000) Role of breast cancer resistance protein in the bioavailability and fetal penetration of topotecan. *J Natl Cancer Inst* 92:1651–1656.

Kruijtzer CM, Beijnen JH, Rosing H, ten Bokkel Huinink WW, Schot M, Jewell RC, Paul EM, and Schellens JH (2002) Increased oral bioavailability of topotecan in combination with the breast cancer resistance protein and P-glycoprotein inhibitor GF120918. *J Clin Oncol* 20:2943–2950.

Kullak-Ublick GA, Fisch T, Oswald M, Hagenbuch B, Meier PJ, Beuers U, and Paumgartner G (1998) Dehydroepiandrosterone sulfate (DHEAS): identification of a carrier protein in human liver and brain. *FEBS Lett* 424:173–176.

Kusuhara H and Sugiyama Y (2001) Efflux transport systems for drugs at the blood-brain barrier and blood-cerebrospinal fluid barrier (part 1). *Drug Discov Today* 6:150–156.

Leggas M, Adachi M, Scheffer GL, Sun D, Wielinga P, Du G, Mercer KE, Zhuang Y, Panetta JC, Johnston B, et al. (2004) Mrp4 confers resistance to topotecan and protects the brain from chemotherapy. *Mol Cell Biol* 24:7612–7621.

Mogi M, Yang J, Lambert JF, Colvin GA, Shiojima I, Skurk C, Summer R, Fine A, Quesenberry PJ, and Walsh K (2003) Akt signaling regulates side population cell phenotype via Bcrp1 translocation. *J Biol Chem* 278:39068–39075.

Murakami H, Takanaga H, Matsuo H, Ohtani H, and Sawada Y (2000) Comparison of blood-brain barrier permeability in mice and rats using in situ brain perfusion technique. *Am J Physiol Heart Circ Physiol* 279:H1022–H1028.

Schinkel AH, Smit JJ, van Tellingen O, Beijnen JH, Wagenaar E, van Deemter L, Mol CA, van der Valk MA, Robanus-Maandag EC, te Riele HP, et al. (1994) Disruption of the mouse mdr1a P-glycoprotein gene leads to a deficiency in the blood-brain barrier and to increased sensitivity to drugs. *Cell* 77:491–502.

Schinkel AH, Wagenaar E, Mol CA, and van Deemter L (1996) P-glycoprotein in the blood-brain barrier of mice influences the brain penetration and pharmacological activity of many drugs. *J Clin Investig* 97:2517–2524.

Schumacher M, Guennoun R, Robel P, and Baulieu EE (1997) Neurosteroids in the hippocampus: neuronal plasticity and memory. *Stress* 2:65–78.

Stoffel-Wagner B (2001) Neurosteroid metabolism in the human brain. *Eur J Endocrinol* 145:669–679.

Sun H, Dai H, Shaik N, and Elmquist WF (2003) Drug efflux transporters in the CNS. *Adv Drug Deliv Rev* 55:83–105.

Suzuki M, Suzuki H, Sugimoto Y, and Sugiyama Y (2003) ABCG2 transports sulfated conjugates of steroids and xenobiotics. *J Biol Chem* 278:22644–22649.

Takasato Y, Rapoport SI, and Smith QR (1984) An in situ brain perfusion technique to study cerebrovascular transport in the rat. *Am J Physiol* 247:H484–H493.

van Aubel RA, Smeets PH, Peters JG, Bindels RJ, and Russel FG (2002) The MRP4/ABCC4 gene encodes a novel apical organic anion transporter in human kidney proximal tubules: putative efflux pump for urinary cAMP and cGMP. *J Am Soc Nephrol* 13:595–603.

van Herwaarden AE, Jonker JW, Wagenaar E, Brinkhuis RF, Schellens JH, Beijnen

JH, and Schinkel AH (2003) The breast cancer resistance protein (Bcrp1/Abcg2) restricts exposure to the dietary carcinogen 2-amino-1-methyl-6-phenylimidazo[4,5-b]pyridine. *Cancer Res* 63:6447–6452.

Weill-Engerer S, David JP, Sazdovitch V, Liere P, Eychenne B, Pianos A, Schumacher M, Delacourte A, Baulieu EE, and Akwa Y (2002) Neurosteroid quantification in human brain regions: comparison between Alzheimer's and nondemented patients. *J Clin Endocrinol Metab* 87:5138–5143.

Zelcer N, Reid G, Wielinga P, Kuil A, Van Der Heijden I, Schuetz JD, and Borst P (2003) Steroid- and bile acid-conjugates are substrates of human MRP4 (ABCC4). *Biochem J* 371:361–367.

Zhang W, Mojsilovic-Petrovic J, Andrade MF, Zhang H, Ball M, and Stanimirovic DB (2003) Expression and functional characterization of ABCG2 in brain endothelial cells and vessels. *FASEB J* 17:2085–2087.

Zhang Y, Han H, Elmquist WF, and Miller DW (2000) Expression of various multidrug resistance-associated protein (MRP) homologues in brain microvessel endothelial cells. *Brain Res* 876:148–153.

Address correspondence to: Dr. Yuichi Sugiyama, Department of Molecular Pharmacokinetics, Graduate School of Pharmaceutical Sciences, The University of Tokyo, 7-3-1 Hongo, Bunkyo-ku, Tokyo, 113-0033, Japan. E-mail: sugiyama@mol.f.u-tokyo.ac.jp

0013-7227/04/$15.00/0
Printed in U.S.A.

Endocrinology 145(9):4384–4391

doi: 10.1210/en.2004-0058

Involvement of Multispecific Organic Anion Transporter, Oatp14 (*Slc21a14*), in the Transport of Thyroxine across the Blood-Brain Barrier

KIMIO TOHYAMA, HIROYUKI KUSUHARA, AND YUICHI SUGIYAMA

Department of Molecular Pharmacokinetics, Graduate School of Pharmaceutical Sciences, University of Tokyo, Tokyo 113-0033, Japan

The present study was aimed at investigating the involvement of mouse organic anion transporting polypeptide 14 (mOatp14) in the uptake of T_4 across the blood-brain barrier. Functional expression of mOatp14 in HEK293 cells revealed that T_4 and rT_3 are high affinity substrates of mOatp14 (Michaelis constant, 0.34 and 0.46 μM, respectively), and the specific uptake of T_3 was 4-fold less than that of T_4 and rT_3. Taurocholate, probenecid, and estrone-3-sulfate were moderate inhibitors for mOatp14, whereas digoxin (substrate of Oatp2), benzylpenicillin (substrate of Oat3), and large neutral amino acids had no effect. mOatp14 is widely expressed throughout the brain, except for the cerebellum. The expression of mOatp14 in the isolated brain capillaries and the choroid plexus was shown by Western blot. The uptake clearance of T_4 by the cerebral cortex determined using the *in situ* brain perfusion technique in mice was 580 μl/min·g tissue, 3-fold greater than that by the cerebellum, and a saturable component (Michaelis constant, 1.0 μM) accounts for the major fraction of the total uptake. Taurocholate inhibited the uptake of T_4 by the cerebral cortex completely, but the inhibition by estrone-3-sulfate was partial (50%). These results suggest that transporters play a predominant role in the delivery of T_4 to the brain, and mOatp14 accounts for estrone-3-sulfate inhibitable fraction, at least partly. The absence of inhibition by digoxin, benzylpenicillin, leucine, and 2-aminobicyclo-(2,2,1)-heptane-2-carboxylic acid for the uptake of T_4 by the cerebral cortex suggests the presence of other unknown transporter for T_4 uptake by the brain. Immunohistochemical staining revealed basolateral localization of mOatp14 in the choroid plexus in which it may also play a role in T_4 uptake. (*Endocrinology* 145: 4384–4391, 2004)

THYROID HORMONE IS critically involved in development and function of the central nervous system. Severe hypothyroidism during the neonatal period leads to structural alterations, including hypomyelination and defects in cell migration and differentiation, with long-lasting and irreversible effects on behavior and performance, whereas severe hyperthyroidism leads to a series of clinical manifestations, including neurologic and psychiatric symptoms (1). In adults, a number of neurological and psychological symptoms, which can be corrected by proper adjustment of the circulatory thyroid hormones, develops depending on the alterations in thyroid state (2).

The thyroid hormones are produced by the thyroid gland. L-T4, the prehormone, is the major form in the circulating blood and is converted to the active form, T_3, by the iodothyronine-deiodinase in peripheral organs. T_3 exerts its action through the nuclear receptors and regulates the expression of genes, such as nerve growth factor, tropomyosin-related kinase A (trkA), and common neutrotrophin receptor p75 ($p75^{NTR}$), in the brain (3). It has been proposed that serum-free T_4 and T_3 concentrations correlate with the activity level of thyroid hormone-dependent processes (free hormone hypothesis) (4). To exert their effect in the central nervous system, free thyroid hormones in the circulating blood have to cross the barriers of central nervous systems, the blood-brain (BBB) and the blood-cerebrospinal fluid barriers formed by the brain capillary endothelial cells and choroid plexus epithelial cells, respectively. Dratman and colleagues (5, 6) investigated the contribution of the transport via these pathways to thyroid hormone delivery to the central nervous system using autoradiography. The distribution of radioactivity associated with T_4, T_3, and rT_3 was limited to the circumventricular organs after intracerebroventricular administration, and so the transport across the BBB is considered to be a major pathway for the delivery of thyroid hormones in the circulating blood to regions of the brain (5, 6).

BBB is formed by brain capillary endothelial cells, which are characterized by highly developed tight junctions and a paucity of fenestra and pinocytotic vesicles. Due to these characteristics, they act as a physical barrier to separate the brain extracellular fluid from the circulating blood. Pardridge (7) demonstrated saturable uptake of T_3 by the brain using the intracarotid injection method (Brain Uptake Index method) and suggested that there is a specific transport mechanism for T_3 at the BBB. However, the transport mechanism for T_4 across the BBB remains controversial. The uptake of T_4 by the brain has been reported to be saturable in dogs (8) but nonsaturable in mice (9). The reason for this discrepancy remains unknown.

Abbreviations: BBB, Blood-brain barrier; BCH, 2-aminobicyclo-(2,2,1)-heptane-2-carboxylic acid; dpm, decay per minute; $E_2$17βG, 17β-estradiol-D-17β-glucuronide; E-sul, estrone-3-sulfate; K_i, inhibition constant; K_m, Michaelis-Menten constant; Leu, leucine; MCT8, monocarboxylate transporter 8; mOatp14, mouse Oatp14; Oatp14, organic anion transporting polypeptide 14; rOatp14, rat Oatp14; V_{brain}, volume of brain distribution; V_{max}, maximum uptake rate.

Endocrinology is published monthly by The Endocrine Society (http://www.endo-society.org), the foremost professional society serving the endocrine community.

Recently organic anion transporting polypeptide 14 (Oatp14; *Slc21a14*) has been cloned from the rat brain cDNA library using gene microarray techniques by comparing the gene-expression profile of cDNA from the brain capillary with that from the liver and kidney (10). Oatp14 was highly enriched in the brain capillary, compared with brain homogenate, liver, and kidney (10, 11). Functional expression of OATP-F, the human ortholog of Oatp14, revealed that T_4 and the inactive metabolite, rT_3, are high-affinity substrates (12), and rOatp14 accepts amphipathic organic anions, such as cerivastatin, 17β-estradiol-D-17β-glucuronide ($E_2$17βG), and troglitazone sulfate as substrates in addition to T_4 and rT_3 (11). The transport activity of T_3 by OATP-F and rOatp14 was small, compared with that of T_4 and rT_3. Because the expression level of rOatp14 is controlled by the plasma thyroid hormone concentrations (11), it has been hypothesized that rOatp14 is involved in the uptake of thyroid hormones by the brain. There are additional candidate transporters for the transport of thyroid hormones at the brain: Oatp2, another isoform of the Oatp family, large neutral amino acid transporters, and monocarboxylate transporter 8 (MCT8) (13–17). The present study is aimed at investigating whether mOatp14 is involved in the brain uptake of T_4 across the BBB. Stable transformants of mOatp14 were established to reveal the spectrum of inhibitors. The *in situ* brain perfusion technique was carried out to investigate the uptake of T_4 across the BBB, and the effect of inhibitors for mOatp14, Oatp2, and neutral amino acid transporter was examined to reveal the contribution of mOatp14.

Materials and Methods

Chemicals

L-[^{125}I]T_4, [^{3}H]$E_2$17βG, [^{3}H]estrone-3-sulfate (E-sul), [^{125}I]rT_3, and [^{125}I]T_3 were purchased from PerkinElmer Life Science (Boston, MA). [^{14}C]sucrose was purchased from Moravek Biochemicals (Brea, CA). All other chemicals and reagents were of analytical grade and readily available from commercial sources. Before the experiments the purity check of labeled T_4, T_3, and rT_3 was performed using HPLC. HPLC conditions were as follows: column, HPLC column (4 mm; YMC, Kyoto, Japan), 4.6 mm inner diameter × 15 cm; mobile phase 0.2% phosphate buffer/methanol (50/50); rate, 1 ml/min; column temperature, 30 C (18). T_4, T_3, rT_3, and 3,5-T_2 can separate under these conditions.

Animals

Adult male ddY mice (28–35 g, 7–8 wk old) were obtained from Japan SLC, Inc (Shizuoka, Japan). All the animals used throughout this study had free access to food and water. The animal experiments were approved by the Institution Animal Care Committee (Graduate School of Pharmaceutical Science, The University of Tokyo), and performed according to its guidelines.

Cloning of mouse Oatp14 (mOatp14) cDNA and construction of a stable transfectant

Based on the nucleotide sequence reported by Okazaki *et al.* (GenBank accession no. NM_021471), the cDNA encoding a full open reading frame of mOatp14 was cloned from mouse brain cDNA using PCR. The mOatp14 cDNA was subcloned into pcDNA3.1(+) (Invitrogen, Carlsbad, CA) and transfected into HEK293 cells by lipofection with FuGENE6 (Roche Diagnostics, Basel, Switzerland) according to the manufacturer's protocol. The transfectants were selected by culturing them in the presence of G418 sulfate (800 μg/ml) (Gibco BRL, Gaithersburg, MD). The transfectants were maintained in DMEM (Gibco) supplemented with 10% fetal bovine serum, 1% antibiotic-antimycotic (Gibco), and G418 sulfate (400 μg/ml) at 37 C with 5% CO_2 and 95% humidity.

Transport study

Uptake was initiated by adding the radiolabeled ligands to the incubating buffer in the presence and absence of inhibitors after cells had been washed twice and preincubated with Krebs-Henseleit buffer at 37 C for 15 min. The Krebs-Hensleit buffer consisted of 23.8 $NaHCO_3$, 118 NaCl, 4.83 KCl, 1.2 $MgSO_4$, 0.96 KH_2PO_4, 1.53 $CaCl_2$ 5 D-glucose, and 12.5 HEPES (millimoles) adjusted to pH 7.4. The uptake was terminated at designated times by adding ice-cold buffer, and cells were washed three times. The radioactivity associated with cell and medium specimens was determined in a liquid scintillation counter and γ-counter. Ligand uptake is given as the cell-to-medium concentration ratio determined as the amount of ligand associated with the cells divided by the medium concentration. Specific uptake was obtained by subtracting the uptake of vector-transfected cells from that by mOatp14-HEK.

In situ brain perfusion

In situ brain perfusion was carried out according the previous report by Dagenais *et al.* (19). Briefly, mice were anesthetized by ip injection of pentobarbital sodium (50 mg/kg), and the right common carotid artery was catheterized with polyethylene tubing (0.2 mm inner diameter × 0.5 mm outer diameter) mounted on a 30-gauge needle. Before insertion of the catheter, the common carotid artery was ligated caudally. During surgery, body temperature was maintained with a heated plate. The syringe containing the perfusion fluid was placed in an infusion pump (Packard Instruments, Meriden, CT) and connected to the catheter. Before perfusion, the thorax of the animal was opened, the heart was cut, and perfusion was started immediately at a flow rate of 1.0 ml/min. The perfusion fluid consisted of Krebs-Henseleit bicarbonate buffer (millimoles): 25 $NaHCO_3$, 118 NaCl, 4.7 KCl, 1.2 $MgSO_4 \cdot 7H_2O$, 1.2 $NaH_2PO_4 \cdot 2H_2O$, 1.2 $CaCl_2 \cdot 2H_2O$, and 10 D-glucose. The perfusion was gassed with 95% O_2 and 5% CO_2 for pH control (7.4) and warmed to 37 C in a water bath. The perfusate contained a vascular space marker ([^{14}C]sucrose) of 2 μCi/ml and perfusion was terminated by decapitation of a number of the animals at selected times. The brain was removed, and the cortex of the right cerebral hemisphere was placed in a tared vial and weighed. The radioactivity associated with the brain and perfusion fluid specimens was determined in a liquid scintillation counter.

Brain vascular volume was estimated from the tissue distribution of [^{14}C] sucrose, which is known to diffuse very slowly across the BBB, using the following equation:

$$V_{vasc} = X^*/C^*_{perf}$$

where X* [dpm (decay per minute) per gram brain] is the amount of sucrose measured in the right cortex and C^*_{perf} (dpm per minute per microliter) is the concentration of labeled sucrose in the perfusate. The apparent volume of brain distribution (V_{brain}) was calculated from the amount of radioactivity in the right cortex using the following equation:

$$V_{brain} = X_{brain}/C_{perf}$$

where X_{brain} (dpm per gram brain) is the amount of tracer measured in the right cortex and C_{perf} (disintegrations per minute per microliter) is the concentration of labeled tracer in the perfusate. Brain tissue radioactivity was corrected for vascular contamination using the following equation:

$$X_{brain} = X_{tot} - V_{vasc}{}^*C_{perf}$$

where X_{tot} (dpm per gram brain) is the total quantity of tracer measured in the tissue sample.

The initial uptake clearance was calculated from the following equation:

$$CL_{up} = V_{brain}/T$$

where T is the perfusion time (minutes).

Kinetic analysis

Kinetic parameters were obtained from the following (Michaelis-Menten) equation:

$$v = V_{max} * S/(K_m + S)$$

where v is the uptake rate of the substrate (picomoles per minute per milligram protein), S is the substrate concentration in the medium (micromoles), K_m is the Michaelis-Menten constant (micromoles), and V_{max} is the maximum uptake rate (picomoles per minute per milligram protein). The experimental data were fitted to the equation by nonlinear regression analysis with weighting as the reciprocal of the observed values using the MULTI program, and the Damping Gauss Newton method algorithm was used for fitting (20).

Inhibition constants (K_i) for mOatp14-mediated transport were calculated from the following equation assuming competitive inhibition:

$$v_{+inhibitor}/v = 1/(1 + I/K_i)$$

where $v_{+inhibitor}$ is the uptake rate of the substrate inhibited by ligands (picomoles per minute per milligram protein) and I is the inhibitor concentration in the medium (micromoles).

Capillary isolation

The method of capillary isolation was described by Ball *et al.* (21) and Dallaire *et al.* (22). Capillary isolation was performed by using the modified method. Briefly, the cortex was homogenized in 0.32 M sucrose (ratio 1 g brain/20 ml sucrose) using a Polytron homogenizer. The homogenate was centrifuged at 4 C at 2200 × *g* for 10 min, and the resulting pellet was suspended in 25% BSA and centrifuged at 4 C at 2200 × *g* for 10 min. The supernatant was decanted, and the pellet was washed three times with buffer: 10 mM Tris-Cl, 0.5 mM dithiothreitol (pH 7.6). The purity of the brain capillary enrichment fraction was examined by estimating the γ-GTP activity.

Northern blot analysis

A commercially available hybridization blot containing poly A+ RNA from various mouse tissues (mouse MTN blot, CLONTECH, Palo Alto, CA) was used for the Northern blot analysis. A fragment (position numbers 86–841) from mOatp14-ORF was used as a probe. The master blot filter was hybridized in Perfecthyb Plus (Sigma, St. Louis, MO) with the ^{32}P-labeled probe at 68 C according to the manufacturer's instructions. Finally, the filter was washed under high stringency conditions (0.1× saline sodium citrate: 0.15 M NaCl and 0.015 M sodium citrate) and 0.1% sodium dodecyl sulfate at 65 C.

Western blot analysis

Antiserum against the carboxyl-terminal of rat Oatp14 (rOatp14) (11) was available for mOatp14. The specimens were loaded onto a 10% SDS-PAGE with a 3.75% stacking gel. Proteins were electroblotted onto a polyvinylidene difluoride membrane (Pall, Port Washington, NY). The membrane was blocked with Tris-buffer saline containing 0.05% Tween 20 and 3% skimmed milk for 1 h at room temperature. After incubation with the primary antibody, detection was carried out by binding a horseradish peroxidase-labeled antirabbit IgG antibody (Amersham Bioscience, Buckinghamshire, UK). Regional difference of mOatp14 was examined using mouse multiple brain tissue region-specific blots (Geno Technology, St. Louis, MO).

Immunohistochemical staining

Adult mice were perfused with 4% paraformaldehyde/PBS. The cerebrum was isolated and stored in 4% paraformaldehyde/PBS for 2 h at 4 C. Before sectioning, the cerebrum was immersed in 20% sucrose at 4 C. Cryostat sections (10 μm thick) were fixed in methanol at −20 C for 10 min, washed with PBS, and blocked with 1% BSA/PBS at room temperature for 4 h, and then primary antibodies (rabbit anti-rOatp14 serum (1:100 dilution in 1% BSA/PBS) and C219 (1:40 dilution in 1% BSA/PBS) were kept at 4 C for 44 h. For detection of the signals, sections were incubated with secondary antibodies (Alexa Fluor 568 antirabbit IgG and Alexa Fluor 488 antimouse IgG, diluted to 1:200; Molecular Probes, Eugene, OR) for 1 h, and the nucleic acid was simultaneously stained with TO-PRO-3 iodide (Molecular Probes) and mounted in Vectashield mounting medium (Vector Laboratories, Burlingame, CA).

Results

Transport properties of mOatp14

Figure 1, A–E, shows the time profiles of the uptake of [^{125}I]L-T4, [^{125}I]rT_3, [^{3}H]$E_2$17βG, [^{125}I]T_3, and [^{3}H]E-sul by

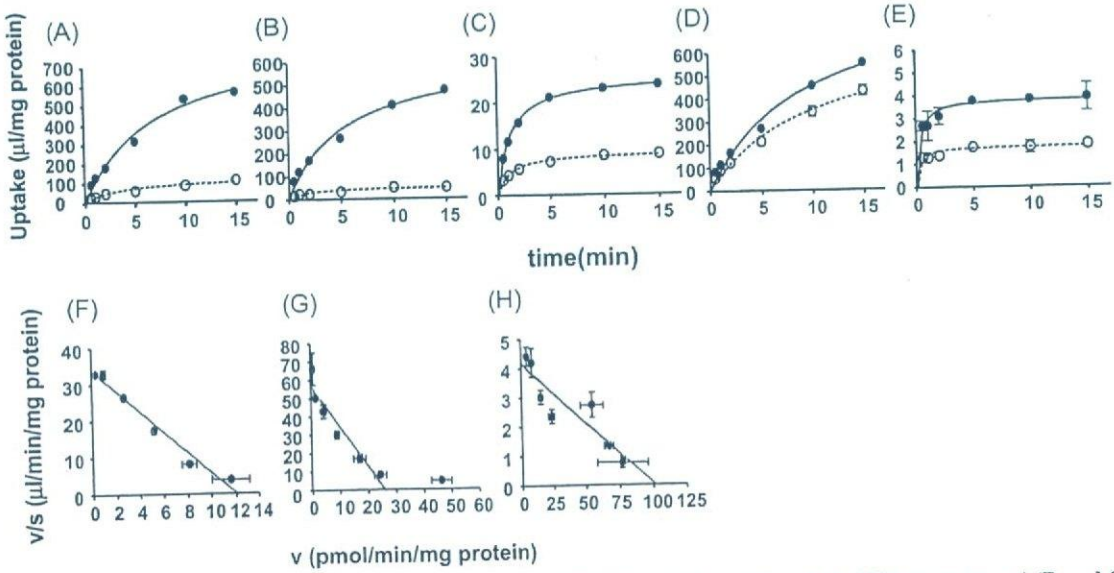

FIG. 1. Time profiles and concentration dependence of the uptake of [^{125}I]L-T4 (0.01 μM) (A and F), [^{125}I]rT_3 (0.01 μM) (B and G), [^{3}H]$E_2$17βG (1 μM) (C and H), [^{125}I]T_3 (0.01 μM) (D), and [^{3}H]E-sul (1 μM) (E) by mOatp14-HEK. The uptake by mOatp14-HEK was examined at 37 C. The *upper figures* (A–E) show the time profiles. *Closed* and *open circles* represent the uptake by mOatp14-transfected HEK293 cells and vector-control cells, respectively. The *lower figures* (F–H) show the concentration dependence as an Eadie-Hofstee plot. Specific uptake was obtained by subtracting the uptake by vector-control cells from that by mOatp14-HEK. The *solid line* represents the fitted line. Each *point* represents the mean ± SE (n = 3).

mOatp14-expressed HEK293 cells and vector-control cells. Specific uptake of [^{125}I]L-T4, [^{125}I]rT_3, and [^{3}H]$E_2$17βG by mOatp14-HEK was observed, whereas the uptake of [^{125}I]T_3 and [^{3}H]E-sul by mOatp14-HEK was slightly greater than that by vector transfected cells. The mOatp14-mediated $E_2$17βG uptake increased linearly over 2 min, whereas that of T_4 and rT_3 increased linearly over 5 min. The mOatp14-mediated uptake followed Michaelis-Menten kinetics (Fig. 1, F–H). The kinetic parameters for the uptake by mOatp14 were determined by nonlinear regression analysis and are summarized in Table 1.

The *cis*-inhibitory effect of thyroid hormones, their related compounds, and organic anions on the mOatp14-mediated uptake of [^{125}I]L-T4 was examined. D-T4, rT_3, and 3,3′,5-triiodothyroacetic acid were potent inhibitors of mOatp14, T_3, taurocholate, E-sul, $E_2$17βG, and probenecid were moderate inhibitors (Fig. 2), whereas 3,5-T2, digoxin, benzylpenicillin, and leucine (Leu) had no inhibitory effect on mOatp14-mediated transport (data not shown). The respective Ki values are summarized in Table 2.

TABLE 1. K_m, V_{max}, and V_{max}/K_m values for mOatp14-mediated transport

Substrate	K_m (μM)	V_{max} (pmol/min·mg protein)	V_{max}/K_m (μl/min·mg protein)
T_4	0.34 ± 0.03	11.7 ± 0.7	34.0 ± 3.5
rT_3	0.46 ± 0.08	25.5 ± 3.0	55.1 ± 11.4
$E_2$17βG	23.5 ± 5.2	95.8 ± 14.6	4.07 ± 1.09

The kinetic parameters for mOatp14-mediated transport were determined by nonlinear regression analysis. Results represent the mean ± SE. The data are taken from Fig. 4, A–C.

Tissue distribution of mOatp14

The tissue distribution of mOatp14 was determined by Northern blot analysis. The hybridization signal was detected predominantly in the brain at approximately 3.5 kb (Fig. 3A). The distribution of mOatp14 in the brain was examined by Western blot analysis. There were two bands nearly the expected size. The band with the greater molecular mass was detected almost ubiquitously but not in the cerebellum (Fig. 3C). Because the mRNA of mOatp14 was not detected in the cerebellum by RT-PCR (data not shown), the band detected at the lower molecular weight in the cerebellum is unlikely to be associated with mOatp14. The expression of mOatp14 in the choroid plexus-, brain homogenate-, and brain capillary-enriched fraction was examined by Western blot analysis. The enrichment factor of γGTP of the isolated brain capillary-enriched fraction was 10.7. Immunoreactive protein was detected at approximately 90,000 in the

TABLE 2. K_i values for mOatp14

Substrate	K_i (μM)	
	This study	Sugiyama *et al.* (11)
rT_3	0.91 ± 0.21	ND
D-T_4	0.27 ± 0.04	ND
T_3	24.2 ± 9.7	2.46 ± 0.96
Triac	2.15 ± 0.50	ND
$E_2$17βG	>100	ND
Probenecid	293 ± 115	39.5 ± 8.3
Estron-3-sulfate	53.1 ± 7.4	6.63 ± 1.62
Taurocholate	109 ± 32	7.24 ± 3.33

The K_i values (this study) were determined for the uptake of T_4 by mOatp14-HEK by nonlinear regression analysis. The data are taken from Fig. 6, A–H. Results represent the mean ± SE. The K_i values for the uptake of $E_2$17βG by rOatp14-HEK were cited from Sugiyama *et al.* (11). 3,5-T_2, benzylpenicillin, PAH, digoxin, Tyr, Leu, Trp, Phe had no effect. ND, Not determined.

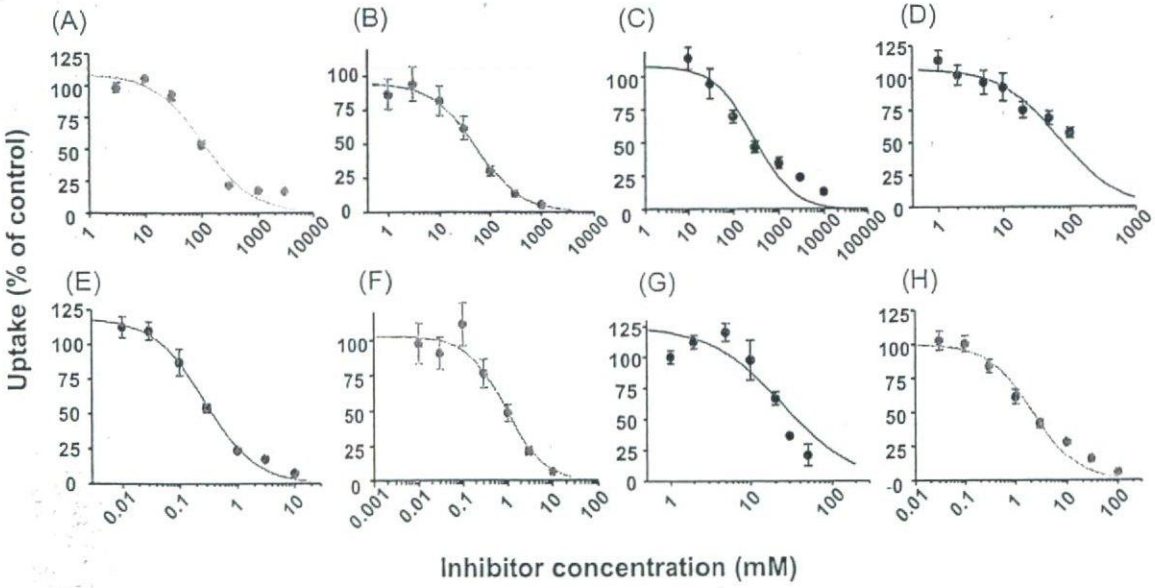

FIG. 2. Inhibition of the uptake of [^{125}I]L-T4 by mOatp14-HEK. The uptake of [^{125}I]L-T4 by mOatp14-HEK was determined in the presence and absence of inhibitors [taurocholate (A), E-sul (B), probenecid (C), $E_2$17βG (D), D-T4 (E), rT_3 (F), T_3 (G), and 3,3′,5-triiodothyroacetic acid) (H)] at the concentrations indicated. The specific uptake was obtained by subtracting the uptake by vector-control cells from that by mOatp14-HEK. The *solid line* represents the fitted line obtained by nonlinear regression analysis. Each *point* represents the mean ± SE (n = 3).

choroid plexus-, brain homogenate-, and the isolated brain capillary-enriched fraction. The signal of the brain capillary band was stronger than that of the brain homogenate (Fig. 3B).

The membrane localization of mOatp14 at choroid plexus was examined by immunohistochemical staining using frozen sections of mouse brain. The signal associated with mOatp14 (*red*) was detected at the basolateral membrane of the choroid plexus epithelial cells (Fig. 3D).

In situ brain perfusion

The time profile of the uptake of [^{125}I]L-T4 by the brain (cortex and cerebellum) is shown in Fig. 4A. The uptake clearance by the cerebral cortex was 3-fold greater than that by the cerebellum (583 ± 71 *vs.* 185 ± 27 μl/min·g tissue) (Fig. 4B). The distribution volume of sucrose was 11.8 ± 0.5 and 19.2 ± 1.5 μl/g tissue for the cerebral cortex and cerebellum, respectively. The following experiments were performed for the brain uptake determined at 60 sec. The uptake by the cerebral cortex was saturable in mice (Fig. 5). The Km, Vmax, and clearance corresponding to the nonsaturable components of [^{125}I]T4 uptake by the cerebral cortex were 1.02 ± 0.16 μM, 423 ± 65 pmol/min·mg protein, and 15.6 ± 7.8 μl/min·g tissue, respectively. However, the fraction of saturation was smaller for the uptake of T_4 by the cerebellum (140 ± 30 *vs.* 44.8 ± 4.6 μl/min·g tissue at 0.01 and 10 μM, respectively). The uptake of [^{125}I]L-T4 by the cerebral cortex was inhibited markedly by taurocholate and partly by E-sul, whereas Leu, 2-aminobicyclo-(2,2,1)-heptane-2-carboxylic acid (BCH), benzylpenicillin, and digoxin had no effect. $E_2$17βG had a weak inhibitory effect (Fig. 6).

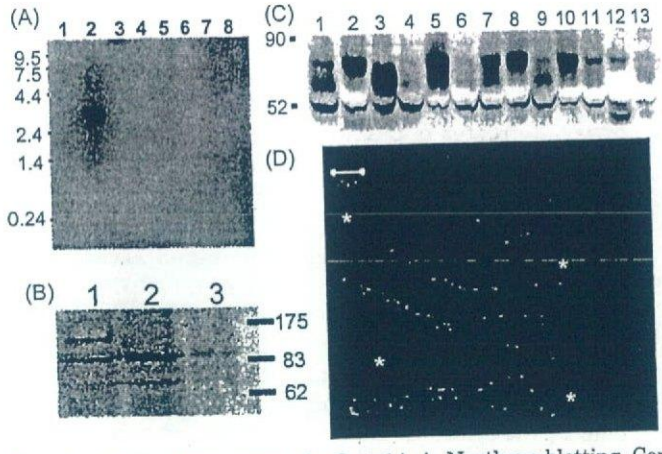

FIG. 3. Tissue distribution of mOatp14. A, Northern blotting. Commercially available mouse multiple tissue Northern blots containing 2 μg poly(A)+ RNA were hybridized for 3 h using the Oatp14 fragment as a probe. Lane 1, Heart; lane 2, brain; lane 3, spleen; lane 4, lung; lane 5, liver; lane 6, skeletal muscle; lane 7, kidney; lane 8, testis. B, Western blotting. Lane 1, Brain homogenate (30 μg); lane 2, the isolated brain capillary-enriched fraction (30 μg); lane 3, choroid plexus (two mice). These proteins were separated by SDS-PAGE (10% separating gel). Oatp14 was detected by Oatp14 polyclonal antibody. C, Western blotting. Each lane of commercially available mouse multiple brain tissue region-specific blots contained 75 μg protein. Lane 1, Frontal cortex; lane 2, posterior cortex; lane 3, cerebellum; lane 4, hippocampus; lane 5, olfactory bulb; lane 6, striatum; lane 7, thalamus; lane 8, midbrain; lane 9, entorhinal cortex; lane 10, pons; lane 11, medulla; lane 12, spinal cord; lane 13, total brain. D, Immunohistochemical staining of mOatp14. Frozen sections of mouse brain were single stained with Oatp14 polyclonal antibody (*red*). Nuclei were stained with TO-PRO-3 iodide (*blue*). *Asterisk* indicates the cerebrospinal fluid space.

Discussion

In the present study, mOatp14-mediated uptake was characterized by constructing a stable expression system, and the uptake mechanism of T_4 by the brain was investigated using the *in situ* brain perfusion technique. From the results of the uptake studies, the transport properties of mOatp14 are similar to that of rOatp14. The transport activity of T_4 and rT_3 was much greater than that of T_3, and amphipathic organic anions were accepted as substrates (Fig. 1). Furthermore, the substrate recognition by mOatp14 was investigated by a *cis*-inhibition study using thyroid hormones and related agents (Fig. 2, E–H). Because the Ki value of D-T4 (stereoisomer of L-T4) was similar to the Km value of L-T4, there is no stereosensitivity in the substrate recognition by mOatp14 (Table 2). rT_3 potently inhibited T_4 uptake, whereas T_3 had a 25-fold greater Ki value than T_4 and rT_3, and 3,5-T2 had no effect (Table 2). These results suggest the importance of iodine attached to the outer ring for high-affinity recognition of T_4 and rT_3 by mOatp14.

Probenecid, taurocholate, E-sul, and $E_2$17βG were moderate or weak inhibitors of mOatp14 (Table 2). Digoxin and benzylpenicillin, which are good substrates of Oatp2 and Oat3, respectively, had no effect on the uptake of T_4 by mOatp14, and neutral amino acids (Leu, phenylalanine, tryptophan, and tyrosine) had no effect either (data not shown). The contribution of mOatp14 and other transporters can be

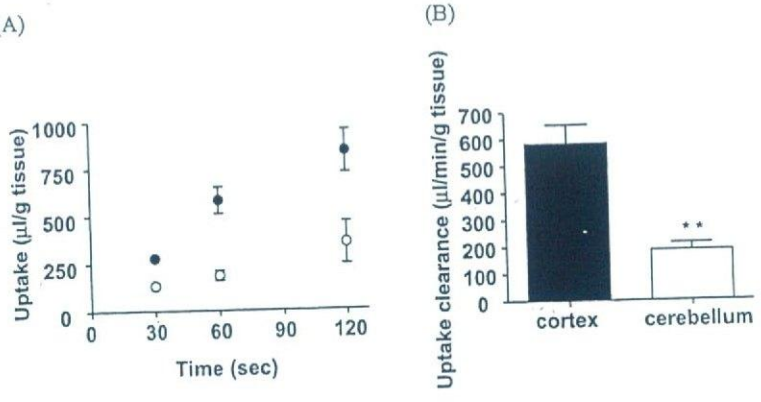

FIG. 4. A, Time profiles of the uptake of [^{125}I]L-T4 by the cerebral cortex and cerebellum. The uptake volume was determined by the *in situ* brain perfusion technique. *Closed* and *open circles* represent the uptake of [^{125}I]L-T4 by the cerebral cortex and cerebellum, respectively. Each *point* represents the mean ± SE (n = 3). B, The initial uptake clearance by the cerebral cortex and cerebellum after 60 sec. Each set of data represents the mean ± SE (n = 3). **, $P <$ 0.01.

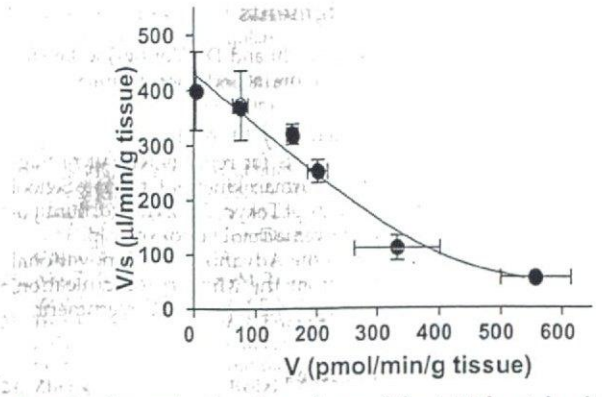

FIG. 5. Concentration dependence of the initial uptake clearance of [^{125}I]L-T4 by the cerebral cortex (concentration 0.01, 0.2, 0.5, 0.8, 10 µm). Each *point* represents the mean ± SE (n = 3). V, Uptake rate of the substrate; s, substrate concentration in the perfusate.

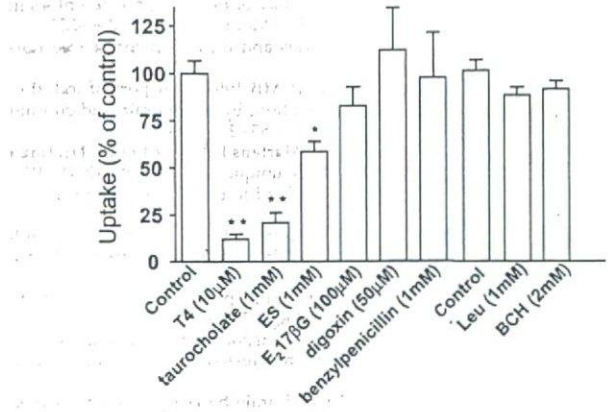

FIG. 6. Inhibition of the uptake of [^{125}I]L-T4 by the cerebral cortex. The uptake was measured in the absence (control, 100%) and presence of T_4 (10 µM), taurocholate (1 mM), E-sul (ES) (1 mM), $E_2$17βG (100 µM), digoxin (50 µM), benzylpenicillin (1 mM), Leu (1 mM), and BCH (2 mM). Each set of data represents the mean ± SE (n = 3–6). **, $P < 0.01$ and *, $P < 0.05$ relative to the corresponding control.

evaluated using these compounds as inhibitors. The Ki values of these compounds for mOatp14 were 10-fold greater than the previously reported values determined for the uptake of $E_2$17βG by rOatp14 (11). There was a discrepancy of more or less 1 order of magnitude in the Ki values of inhibitors for rat and mouse Oatp14, even though they were determined by the same methods, whereas the Km values of T_4 and $E_2$17βG for mOatp14 were comparable with those for rOatp14. Different test substrates were used to determine the Ki values of inhibitors ($E_2$17βG for rOatp14 *vs.* T_4 for mOatp14). Because $E_2$17βG had a lower inhibitory effect on T_4 uptake by mOatp14 than expected from its Km value, the Ki value of $E_2$17βG will be greater than its own Km value. As far as two substrate compounds share the same substrate recognition sites in the transporter, the Ki value of one compound for the uptake of the other should be the same as its own Km value. The discrepancies in the kinetic parameters for different substrates ($E_2$17βG and T_4) suggest that Oatp14 has at least two different substrate recognition sites. Therefore, the difference in the Ki value for the uptake of $E_2$17βG and T_4 by rat and mouse is not ascribed to the species difference but presumably accounted for by multiple recognition sites for T_4 and $E_2$17βG by mOatp14 as reported in rOatp2 (23). The Ki value of $E_2$17βG for the digoxin uptake by rOatp2 (0.04 µM) was much smaller than its Km value (1 µM) (23).

mOatp14 is widely expressed throughout the brain, and strong expression was observed in the posterior cortex, olfactory bulb, thalamus, midbrain and pons, whereas the expression in the cerebellum was below detection. Regional differences have also been observed in human OATP-F, which is not expressed in the cerebellum or pons (12). Li *et al.* (10) and Sugiyama *et al.* (11) demonstrated that rOatp14 is highly enriched in the isolated brain capillaries, and furthermore, Sugiyama *et al.* demonstrated that rOatp14 is expressed at plasma membrane of the brain capillaries in rats by immunohistochemical staining (11).

To investigate an involvement of mOatp14 in the T4 uptake across the BBB, the brain uptake of T_4 was characterized using the *in situ* brain perfusion technique. The uptake of T_4 was 3-fold greater in the cerebral cortex than in the cerebellum (Fig. 4B). A saturable component accounted for about 95% of the total uptake of T_4 by the cerebral cortex, suggesting the important role of transporters in T_4 uptake at the BBB (Fig. 5). The Km value of T_4 uptake at the cerebral cortex was almost comparable with the Km value of mOatp14 (1.02 *vs.* 0.34 µM). T_4 is highly bound to plasma T_4 binding proteins (24). Based on the free hormone hypothesis, in which free T_4 and T_3 concentrations correlate with the activity level of thyroid hormone-dependent processes (4), free T_4 will be taken up by the brain via the specific transport systems at the BBB. For mice, the range of normal serum-free T_4 is approximate 10–20 pM (25), much lower than its Km value (1.02 µM), suggesting that the transport mechanism of T_4 uptake across the BBB is not saturated under physiological conditions. In contrast, in the cerebellum, the fraction of saturation was small. These results are in good agreement with regional differences in the expression of mOatp14. Taurocholate completely inhibited the uptake of T_4 by the cerebral cortex, and E-sul and $E_2$17βG had a weak inhibitory effect. Partial inhibition by E-sul, even at a concentration sufficient to inhibit Oatp14-mediated transport completely, suggests that T_4 uptake across the BBB cannot be fully accounted for by mOatp14, and another transporter is involved in the uptake of T_4 by the cerebral cortex. The Eadie-Hofstee plot indicated that the uptake of T_4 by the brain consists of a single saturable component, suggesting that the unknown transporter has a Km value similar to T_4 with mOatp14. Because digoxin, benzylpenicillin, Leu, and BCH had no effect for the uptake of T_4 by the cerebral cortex, the involvement of Oatp2, Oat3, and large neutral amino acid transporters can be excluded. However, several transporters are identified as thyroid hormone transporters up to now (26, 27), and this time we could not estimate the contribution of some transporters. Further studies are necessary to identify the taurocholate-inhibitable transporter involved in the uptake of T_4 together with mOatp14.

In addition to the brain capillaries, Western blot analysis detected mOatp14 protein in the choroid plexus in which it is located on the basolateral membrane (Fig. 3, B and D). Previously, *in situ* choroid plexus perfusion experiments in